男女比は1：3）．妊娠・出産で難聴が発症または進行することも多い．難聴は一側性の場合もあるが，両側に起こることが多い（片側：両側は1：1）．一側性の難聴でも長期経過のうちに対側に難聴を呈することが多い．

鼓膜が正常で後天性の伝音難聴の場合には耳硬化症を疑う．標準純音聴力検査ではstiffness curveとなることが多い．中・低音域に難聴が大きい聴力型を示すことが多い．耳小骨の固着により骨導閾値が2 kHzを中心に上昇し（Carhart notch），見かけ上混合難聴を呈する．耳小骨筋反射は，初期には逆向きやすい反応がみられ，固着が高度になると消失する．ティンパノグラムはA型またはAs型を示す．感音難聴による感音難聴も出現することがある．側頭骨CTではアブミ骨は正常に描出され，前庭窓前庭に骨透亮像を認めることが多い．蝸牛周囲にわたって骨透亮像が描出されることもある．高度の病変では前庭窓が硬化病変で埋まってしまうこともある．蝸牛型耳硬化症（cochlear otosclerosis）では前述の病変が高度に認められる．

治療方針

有効な薬物療法はない．一般的には手術で伝音難聴の改善をはかる．40 dB以上の難聴で明らかな気骨導差を示す場合が手術のよい適応である．全身状態などから手術を行えない場合や手術を希望しない場合は補聴器を装用する．

Ⓐ手術の分類

アブミ骨の可動をはかる方法とアブミ骨を全摘して（stapedectomy）またはアブミ骨の上部構造を切除してアブミ骨の底板に小穿孔を開け（stapedotomy），代用の人工アブミ骨を用いて再建する方法がある．アブミ骨可動術は再固着の可能性が高く，通常行われない．stapedotomyを選択する施設が多いが，日本人では底板の固着が高度でないためにアブミ骨全体が取れてしまうこともしばしばあり，その場合にはstapedectomyを行う．

Ⓑ手術

外耳道の皮膚を深部でU字型に切開し，鼓膜まで剝離して挙上し，鼓室後方を開放する．鼓索神経を温存しつつ骨性鼓膜輪を可及的に削除してアブミ骨を明視下にする．硬化病変は前庭窓前方に観察できるが，確認できないことも多い．アブミ骨の固着を確認し，ツチ・キヌタ骨の可動性も確認する．キヌタ・アブミ関節を外し，アブミ骨底板に小穿孔を開ける（safety hole）．アブミ骨前後脚とアブミ骨輪靱帯をレーザーで焼灼または切断し，アブミ骨上部構造を摘出する．safety holeを拡大して径0.8 mmに開窓する．長さ約4 mm，径0.6 mmの人工アブミ骨のピストン部分を開窓部に挿入し，他端をキヌタ骨長脚にかけ，耳小骨連鎖を再建する．ピストンの長さはキヌタ骨長脚から開窓部までを実測して選択する．ピストン周囲にgelfoamを置き，外リンパ瘻を予防する．stapedectomyでは結合織を前庭窓のピストン周囲に置く．

Ⓒ人工アブミ骨

人工アブミ骨にはすべてテフロンでできたテフロンピストンと，テフロンとステンレスのワイヤーでできたテフロンワイヤーピストンがある．

Ⓓ成績と合併症

手術成績は良好で95%以上の症例で気骨導差は10 dB以内となり，長期にわたってよい聴力が維持される．術後一過性に眼振を認めることがしばしばあるが，通常1，2日で消失する．時に回転性めまいを数日間訴え，ふらつきが持続することがある．高音域の軽度の感音難聴を術直後に認めることがあるが，通常徐々に回復する．高度な感音難聴の発症はまれである．鼓索神経の一過性の障害により，舌前方の味覚障害を生じることがあるが，通常2，3週間以内に消失する．

患者説明のポイント

・耳硬化症はアブミ骨の固着によって生じる．治療法には手術または補聴器装用がある．手術の聴力改善成績は良好である．感音難聴やめまいなどの合併症が生じる可能性があること，補聴器装用との違いを十分に説明して手術の承諾を得る．

急性感音難聴
acute sensorineural hearing loss

土井勝美　近畿大学教授・耳鼻咽喉科学

病態と診断

急激に発症する感音難聴が急性感音難聴で，急性感音難聴のうち発症原因が明らかなものは突発性難聴と称される．ウイルス感染（ムンプスウイルス・麻疹ウイルスによる聾，帯状疱疹ウイルスによるラムゼイ・ハント症候群）や細菌感染による急性内耳炎，強大音曝露による急性音響外傷（ディスコ難聴），圧外傷・内耳窓破裂を病態とする外リンパ瘻，内耳毒性を有する薬物（アミノグリコシド系抗菌薬・抗癌剤）による薬剤性難聴，聴神経腫瘍や小脳・脳梗塞による中枢性難聴，内リンパ水腫を病態とするメニエール病などがある．

一方で，内耳障害を病態とするものの発症原因が不明の急性感音難聴は突発性難聴と称され，上記の急性感音難聴と突発性難聴との鑑別診断が重要とな

る．また，低音部にのみ急性感音難聴を呈する場合は，急性低音障害型感音難聴と別に分けて診断される．

厚生労働省2001年度調査では，突発性難聴の年間の発症者数は35,000人と報告され，厚生労働省特定疾患急性高度難聴調査研究班の診断基準は，①突然の発症，②高度の感音難聴，③原因不明と定義されている．突発性難聴の病態としては内耳血流障害とウイルス感染が推察されている．

一般的に感音難聴の治療は困難とされているが，突発性難聴は早期に適切な治療を行うことで治癒も期待できる数少ない疾患の1つである．しかしながら，早期治療例でも約20%の症例は治療に無反応で，治療開始が遅れるとさらに治療成績は低下するため，より有効な治療法の開発が望まれている．前庭症状を伴う症例は約30%で，前庭症状のない症例と比較して治療成績は不良の傾向にある．

治療方針

突発性難聴では，発症後1週間以内にステロイドの大量漸減治療を開始することが，よい予後を得るための条件とされる．その他の急性感音難聴の治療も同様で，早期に適切な治療を開始することが重要となる．ウイルス感染が示唆される症例では抗ウイルス薬が併用される．ただし，ムンプス難聴の治療は不能であることが多く，ワクチン接種による難聴発症の予防が重要となる．外リンパ瘻疑い症例では，中耳試験開放により病態の有無を確認し，必要であれば内耳窓閉鎖術を施行する．メニエール病では，浸透圧利尿薬（イソバイド）の投与と併せて，高度の感音難聴に対してステロイドを追加する．急性音響外傷や急性低音障害型感音難聴についてもステロイド治療が基本になる．

ステロイド以外の薬物治療では，血流改善を目的にプロスタグランジン〔PGE_1（プロレナール）・PGI_2（ドルナー）〕，バトロキソビン（DF），ATP（アデホス），アミドトリゾ酸（ウログラフイン），蝸牛神経の賦活化を目的にビタミンB_{12}（メチコバール）が使用される．薬物治療以外では，高圧酸素治療が初期治療として有効とされる．

Ⓐ 点滴治療

Rx 処方例　症状に応じて下記を適宜併用する．

1) 低分子デキストランL注（25 g/250 mL）　1回250 mL　1日1回　点滴静注
2) ソル・コーテフ注（100 mg）　1回500 mgより10日間で漸減　1日1回　点滴静注
3) アデホス-L注　1回60 mg　1日1回　点滴静注
4) メチコバール注　1回500 μg　1日1回　点滴静注

Ⓑ 内服治療

Rx 処方例　病態に応じて下記を組み合わせて用いる．

1) プレドニン錠（5 mg）　6錠より開始，10日間で漸減
   メチコバール錠（500 μg）　3錠
   アデホス顆粒　300 mg（成分量として）
   カルナクリン錠（50単位）　3錠
   （分3）
2) ドルナー錠（20 μg）　3錠　分3 (保外)
3) プロレナール錠（5 μg）　3-6錠　分3 (保外)
4) イソバイドシロップ（70%）　90-120 mL　分3
5) メニレットゼリー（70%）　90 g（製剤量として）　分3

患者説明のポイント

- 早期にステロイドを中心とする適切な治療を行うことで治癒する可能性がある．
- 突発性難聴，メニエール病，外リンパ瘻の鑑別診断は，発症初期には必ずしも容易でなく，経過観察中に診断名・治療法が変更になったり，手術（鼓室試験開放）が必要になることもある．
- 心身の安静に努め，ストレスを回避するよう心掛ける．

突発性難聴

sudden deafness (idiopathic sudden sensorineural hearing loss)

内藤　泰　神戸市立医療センター中央市民病院・副院長

病態と診断

厚生労働省研究班の基準では，主症状として，①突然の難聴，②高度な感音難聴（ただし，明確な基力の基準はない），③原因不明であること，が必とされ，副症状には①耳鳴り，②めまいが挙げる．すべての主・副症状があれば確実例，主症状みなら疑い例になる．聴覚補充現象の有無は一定ず，聴力の改善・悪化の反復はなく，一側性が多が両側例もあり，第8脳神経以外の神経症状はない．

わが国では年間3万-4万人が罹患し，50歳代後半から60歳代前半に発症のピークがある．病因は解明されていないが，内耳の血行障害，ウイルス感染などが想定されている．内耳血行障害説は有力ではあるが，本症が反復しないことが説明しにくい．ウイルス感染では，内耳炎のほかに感染による

STAPES SURGERY AND COCHLEAR IMPLANT SURGERY FOR SEVERE ORTOSCLEROSIS

Katsumi Doi,[1] Mitsuo Sato,[1] Mie Miyashita,[1] Kazuya Saito,[1] Michio Isono,[1] Kyoichi Terao,[1] Izumi Koizuka,[2] Yumi Ohta[3]

[1]Department of Otolaryngology, Kinki University Graduate School of Medicine, Higashiosaka, Osaka, Japan; [2]Department of Otolaryngology, St. Marianna University School of Medicine, Sugao, Kawasaki, Kanagawa, Japan; [3]Department of Otolaryngology, Osaka University Graduate School of Medicine, Osaka, Japan

Introduction

Profound deafness has received increasing attention, because of the availability of cochlear implants (CI). Consequently, it is especially important to remember that a 'blank' audiogram does not necessarily mean absence of hearing. Severe otosclerosis (far-advanced otosclerosis; FAO) generally involves air conduction (AC) levels worse than 85 dB, and bone conduction (BC) levels beyond the limits of the audiometer.[1–4] If AC levels exceed 85 dB but BC levels are measurable at some frequencies but worse than 30 dB, the condition is called advanced otosclerosis (AO). Failure to recognize FAO or AO may result in unnecessary CI surgery.

Materials and methods

A retrospective analysis was conducted of the clinical charts of all patients who received stapes surgery (n = 306) and CI surgery (n = 536) at Osaka and Kinki University Hospitals from 1992 to 2012. Stapes surgery involved 210 ears in females and 96 ears in males. Otosclerosis accounted for 80% of the the stapes surgery. Objective improvement was noted in pure-tone audiogram (PTA), and subjective patients' satisfaction with amplification was the real measure of success because the stapes surgery was performed to restore a serviceable hearing with Hearing aid (HA) for these FAO and AO patients.

Results

Among 306 stapes surgery cases, one patient (NS, 45 years old, male) with FAO received stapedotomy on the right ear, and another patient (MS, 56 years old, male) with AO received bilateral stapedotomy. Both patients had a positive family history of progressive hearing loss. MS's daughter (KM, 28 years old) received partial stapedectomy on the left ear, and the result was excellent. AC levels were worse than 85 dB bilaterally in both patient, and BC levels were not measurable at most (not all) frequencies. The past audiograms and the family history help us to diagnose FAO and AO. Pre-operatively, both patients (NS and MA) were not successful hearing aid (HA) users, although both continued to use a HA anyway. Post-operatively, MS does not need HA any longer, while NS is still wearing HA unsuccessfully and considering CI surgery the left ear.

Among 536 CI surgery cases, just one patient (UH, 52 years old, male) had been found to have the history of otosclerosis preoperatively, and has been a good CI user postoperatively (Fig. 1A). HRCT demonstrated a massive sclerotic lesion bilaterally, indicating the presence of cochlear otosclerosis (Fig. 2A). Past audiograms

Address for correspondence: Katsumi Doi, MD/PhD, 377-2, Oono-Higashi, Osaka-Sayama, 589-8511, Osaka, Japan. kdoi@med.kindai.ac.jp

Cholesteatoma and Ear Surgery – An Update, pp. 000-000
Edited by Harua Takahashi

clearly suggest the presence of an air-bone gap and a progressive nature of HL (Fig. 2B). After cochleostomy onto the promontory, the scala tympani was found to be filled with soft connective tissues. A full insertion of CI24RCS electrodes into the scala vestibuli was successfully completed. Among 2558 CI surgery cases, bilateral otosclerosis accounted for just 1% of the causes of deafness in Japan (Fig. 1B), according to a survey by the Cochlear Corporation in 2006.

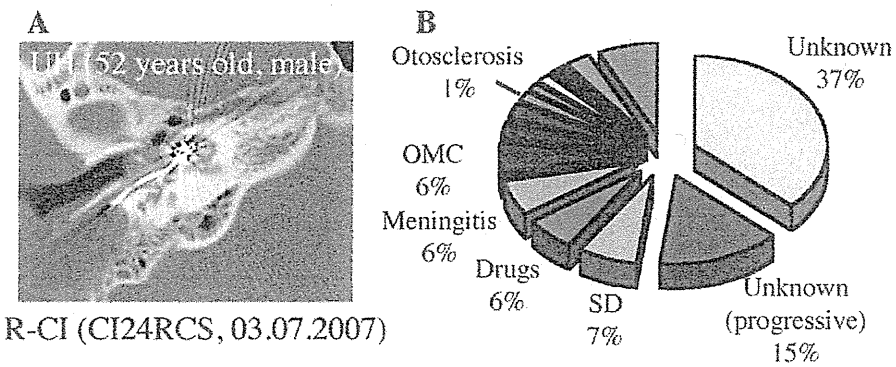

Fig. 1. Profound hearing loss caused by otosclerosis. A: a case of the CI surgery with FAO; B: the causes of deafness in Japanese CI cases (2006).

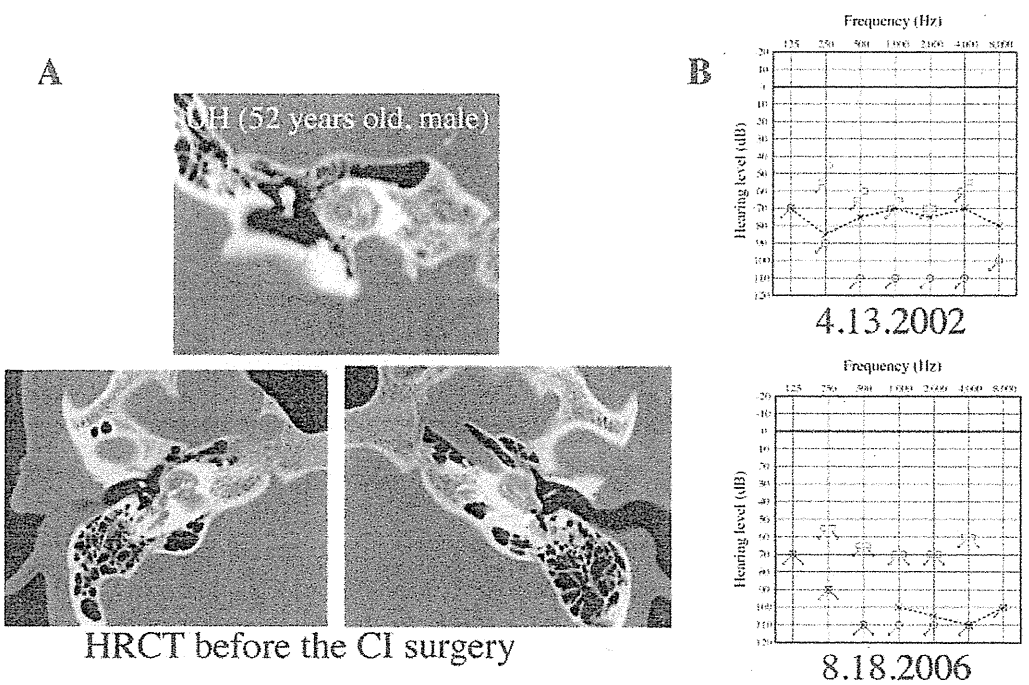

Fig. 2. HRCT and PTA of a patient with FAO who received CI surgery. A: massive sclerotic lesions within bilateral cochlea; B: past audiograms suggesting a progressive hearing loss.

Discussion

A convincing histological explanation for increased bone-conduction threshold in FAO remains an issue for continued investigation. There are two types of otosclerosis described: a conductive disturbance limited to specific areas of the oval and round windows, and a more aggressive form called 'cochlear otosclerosis' with

multiple foci developed relatively early in life. No correlation between BC thresholds and size of the lesion, activity of the lesion, involvement of endosteum or presence of a round window lesion in otosclerosis was found, while moderate diffuse loss of hair cells and cochlear neurons in the basal turn, and strial atrophy near the foci of otosclerosis were reported in FAO patients.

Sheehy[2] published specific diagnostic clues for FAO: 1) positive family history for otosclerosis; 2) progressive hearing loss beginning in early adult life; 3) paracusis during the early stage of the disease; 4) past use of bone-conduction hearing aid; 5) previous audiograms showing an air-bone gap. In addition, the following criteria can be obtained from the physical examination: 1) normal voice; 2) positive Schwarze's sign; 3) evidence of otosclerosis on HRCT; 4) a Weber test lateralizing to the poor ear or a negative Rinne test by a 512-Hz tuning fork; 5) no other apparent cause for hearing impairment. The diagnosis is just presumptive and can be confirmed only at surgery. All of our cases showed a positive family history of hearing loss, a progressive hearing loss on the past audiograms, and sclerotic findings of cochlea on HRCT.

Patients with FAO may appear to be suffering from profound sensorineural hearing loss and are frequently directed to CI programs. Specific clues shown above can lead the clinician to suspect FAO, and some FAO patients who had been unable to use a hearing aid (HA) preoperatively obtained serviceable hearing with a HA after the surgery.[1-4]

The most gratifying aspect of the stapes surgery for severe otosclerosis (FAO and AO) should be converting the patients' hearing from non-serviceable to serviceable with HA. The patients must be aware not only of the risks of the procedure, but also of the relatively limited goals. On the basis of the conventional criteria for stapedectomy surgery, objective results would be sometimes disappointing in FAO. However, some FAO patients clearly do benefit from the surgery and show marked improvement in HA performance. The success rate was reported to range within 70-100%.[1-4] If a successful outcome is not achieved, the patient might be suitable for the CI surgery.

References

1. House HP, Sheehy JL. Stapes surgery; selection of the patient. Ann Otol Rhinol Laryngol 70:1062-1068, 1961
2. Sheehy JL. Surgical correction of far-advanced otosclerosis. Otolaryngol Clin North Am 11:121-123, 1978
3. Glasscock III ME, Storper IS, et al. Stapedectomy in profound cochlear loss. Laryngoscope 106:831-833, 1996
4. Frattali M, Sataloff RT. Far-advanced otosclerosis. Ann Otol Rhinol Laryngol 102:433-437, 1993

あらゆる可能性を考え，薬物療法，補聴器（希望により音響療法）を試み，患者サイドに立った治療の提案を行うことが重要である．

耳閉感

診断

A 病態

耳が塞がったような感じが耳閉感である．外気圧の変化により外気圧と中耳腔の圧が不均衡になった際に感ずる症状で，高い山に登った際，高層ビルのエレベーターに乗った際，トンネルに入った際などに感ずる．外気圧の変化が誘因ではなくこのような耳閉感を感ずる場合，中耳，内耳疾患の存在を疑う．中耳疾患では滲出性中耳炎など種々の中耳炎，耳管狭窄症，耳管開放症などが原因となる．またメニエール病，突発性難聴などの内耳疾患でも耳閉感を生じる．

B 診断

耳閉感は自覚的症状であり，他覚的検査がないのが客観的な診断を困難にしている．鼓膜所見，純音聴力検査のほか，ティンパノメトリー，自記オージオメトリー，SISIテストなどの聴覚検査，耳管機能検査，および画像検査（CT，MRI）を組み合わせ原因となる障害部位診断を行う．

治療方針

原因となる中耳疾患（耳管狭窄症，耳管開放症など），内耳疾患（メニエール病，突発性難聴など）の治療をすることにより症状は軽減する．詳細はそれぞれの疾患の項を参照されたい．

高度難聴（補聴器，人工内耳）

Severe to profound hearing loss (cochlear implant, hearing aid)

内藤　泰　神戸市立医療センター中央市民病院・副院長

診断

一般に平均聴力70 dB以上を高度難聴とよぶことが多い．高度難聴がある場合，聴力検査で難聴の程度を測定するだけでなく，必要に応じて他の聴覚検査，画像診断，遺伝子検査などを駆使し，できる限り難聴の原因まで究明することが大切である．高度難聴では何らかの聴覚補償が必要だが，同程度の難聴でも伝音難聴では補聴の効果が高く，感音難聴では音の神経活動への符号化そのものが障害されるため，補聴器で入力音を増幅しても単純には語音弁別は改善しない．補聴器を装用しても日常生活に大きな障害をきたす場合，入力音の増幅という補聴戦略から蝸牛神経の直接電気刺激，つまり人工内耳という方法に移行する．

小児の高度難聴では，言語という，人として重大な生理機能の発達を扱うため，成人とは別次元の留意が必要である．最初に，補聴器や人工内耳で聴覚を活用する道を歩むのか，手話で言語を獲得するのかという根源的選択が必要であり，主治医は，両親が患児の将来を見据えた最善の判断ができるように，公正な助言ができなければならない．

治療方針

A 補聴器

補聴器装用の適応に絶対的なものはなく，軽度難聴でも学校や職場などでの必要性が高ければ実用上のメリットも大きい．逆に中等度以上の難聴があっても日常生活で必要性を感じない人が仮に補聴器を購入したとしても非使用者になってしまうおそれがある．補聴器の適応判断や機器の選択，装用の具体的指導には，難聴の程度と性質，患者の生活状況，補聴器の性能や特徴について専門的知識を有する補聴器相談医の対応が望ましい．

言語習得前の小児ではことばの発達のために難聴の早期発見と介入が大切で，これには新生児聴覚スクリーニングが大きな役割を果たしている．スクリーニングで要精査となった場合には，各地域で日本耳鼻咽喉科学会認定の精密聴力検査機関が拠点として対応している．乳児で補聴器が必要と判断された場合には6か月ころから装用を開始する．音声言語の習得にはおおむね55 dB以下の補聴器装用閾値が得られることが必要で，これを超えると人工内耳を使用したほうが良好な言語発達が得られる例が多い．

B 人工内耳

本邦の人工内耳適応基準は，成人，小児ともに90 dB以上の難聴で，補聴器の効果が乏しく，内耳が手術可能な状態であることとされ，小児ではこれに，年齢が1歳6か月以上であることと術後の療育体制が整っていることが加わる．

人工内耳手術が可能かどうかについては画像診断が大きな役割をはたす．側頭骨CTで乳突蜂巣発育と軟部組織陰影の有無，顔面神経の位置，内耳の形態，内耳道・蝸牛神経管狭窄の有無などを観察し，MRIで内耳の線維化の有無，蝸牛神経の描出状況や太さなどを評価する．

先天性難聴小児の人工内耳手術は低年齢ほど効果が高いので，補聴器で療育を継続するか人工内耳に進むかの判断は慎重な検査・評価に基づきつつ早期に行うべきである．髄膜炎後失聴例や，遺伝子検査で有効な聴力が期待できないことが明白な症例など

では，漫然と経過を待たずに，より早期の手術も考慮する．人工内耳の装用閾値は25－35 dB程度で，低音から高音域までフラットな効果が得られる．

聴覚医学的には，聴覚補償は両耳のほうが種々の利点がある．人工内耳の使用も基本的にはこれに当てはまるが，補聴器の両耳装用と異なる点として，人工内耳には人工物を手術的に体内に埋め込むことに伴う短期的・長期的リスク，残存聴力損傷の可能性，高額の医療費などの問題もある．先天性高度難聴小児が人工内耳で高い聴覚・音声言語能力を獲得し，社会的に自立した成人になることは，患児本人だけでなく社会全体にも大きなメリットをもたらす．人工内耳の両耳装用について適切な適応基準の確立が望まれる．

また，最近は主に低音域の残存聴力がある症例で正円窓からのアプローチにより，聴力をある程度，場合によってはほぼ完全に保存できるタイプの人工内耳電極も使用可能になってきた．このような例では人工内耳をオフにしても一定の聴覚があり，さらに人工内耳を稼働させることで，騒音下での語音弁別向上など，より高度の聴覚再獲得が可能になる．将来的には，補聴器か人工内耳かという二者択一的な考え方も改めなければならないであろう．

患者説明のポイント

- 高度難聴の診療には時間がかかる．中途失聴者では筆談，小児では両親へのカウンセリングが必要である．十分な診察時間を確保するとともに，言語聴覚士や看護師などと役割を分担してチームで対応すると手厚い説明ができ，患者の疾病理解が深まる．
- 感音難聴では補聴器を使用しても大なり小なり，音が割れたり，やかましく聞こえることは避けがたく，騒音下，反響のある広い場所，多人数との会話などでの聞き取りも難しい．補聴器の限界を理解してうまく使いこなせるように丁寧に説明する．
- 補聴器や人工内耳を使用しても聴覚が正常になるわけではない．特に高度難聴小児が高い音声言語能力を習得するには長期間の専門的指導と日常生活や教育上のさまざまな支援が必要であることを両親に説明する．

看護・介護のポイント

- 難聴者，人工内耳使用者との会話では，静かな場所において1対1で正面から口の動きを大きくして，ゆっくり，はっきり話すように努め，重要事項は筆談や印刷物を併用して正確な理解を確保する．
- 小児難聴の場合，親は子どもが難聴である事実に当惑し，受け入れがたい気持ちになるのが通常である．患児の療育を円滑に推進するうえで，医学的な説明に加えて，親の心情に寄り添い，支援する姿勢が重要である．

めまい，平衡障害
vertigo and dysequilibrium

肥塚　泉　聖マリアンナ医科大学教授・耳鼻咽喉科

病態と診断

めまいには，末梢前庭系の障害による末梢性めまいと，中枢前庭系の障害を原因とし，生命に対する危険性を有す中枢性めまいとがあり，両者の鑑別が重要である．

末梢性めまいには聴覚症状（難聴・耳鳴・耳閉感など）が随伴することが多く，問診の際にこれを確認する．

中枢性めまいの代表格は，Wallenberg症候群などの脳幹・小脳梗塞や小脳出血である．Wallenberg症候群におけるめまいは前庭神経核の虚血により生じるため，末梢性めまいと同様，回転性めまいが生じるので注意が必要である．前庭神経核周辺の神経核も同時に障害され，他の中枢神経症状を伴う．前庭神経核より頭側の虚血の場合，動眼神経核群があり複視を訴える．尾側の虚血では，三叉神経脊髄路核の障害により口囲の痛覚の低下，迷走神経背側運動核の障害により軟口蓋や声帯麻痺，交感神経下行路の障害ではHorner症候群が認められる．複視や口囲のしびれ，構音障害がなかったかを必ず問診し，他覚的にもこれらの症状の有無をチェックすることが重要である．小脳出血は初期にめまい，悪心，嘔吐，頭痛（突然ピーク形）などである．末梢性めまいと紛らわしい症状で発症することがあるので注意を要する．中枢性めまいが疑われる場合はCTやMRIなどを行う．発症6時間以内の脳幹・小脳梗塞超急性期の診断には，MRI（拡散強調画像）が有用である．小脳出血の診断にはCTが有用である．

治療方針

Ⓐ めまい急性期の治療

めまい急性期は悪心や嘔吐などの前庭自律神経反射による症状が強く，これらに対する対症療法が先される．患者にとって一番楽な姿勢をとらせ，外的刺激の少ない静かな暗い部屋で体動をできるだけり避けるようにして安静を保つ．病状を十分に説明して，不安感を取り除くように努める．めまい急性期は内服が困難かつ症状への速効性が要求され

Journal of Controlled Release 157 (2012) 112–117

Contents lists available at ScienceDirect

Journal of Controlled Release

journal homepage: www.elsevier.com/locate/jconrel

Micellization of cisplatin (NC-6004) reduces its ototoxicity in guinea pigs

Miyuki Baba [a,b], Yu Matsumoto [a,b], Akinori Kashio [a], Horacio Cabral [c], Nobuhiro Nishiyama [b], Kazunori Kataoka [b,c,d,e], Tatsuya Yamasoba [a,*]

[a] Department of Otolaryngology and Head and Neck Surgery, Faculty of Medicine, Graduate School of Medicine, Hongo 7-3-1, Bunkyo-Ku, Tokyo, 113–8655, Japan
[b] Division of Clinical Biotechnology, Center for Disease Biology and Integrative Medicine, Graduate School of Medicine, Hongo 7-3-1, Bunkyo-Ku, Tokyo, 113–8655, Japan
[c] Department of Bioengineering, Graduate School of Engineering, Hongo 7-3-1, Bunkyo-Ku, Tokyo, 113–8655, Japan
[d] Department of Materials Engineering, Graduate School of Engineering, Hongo 7-3-1, Bunkyo-Ku, Tokyo, 113–8655, Japan
[e] Center for NanoBio Integration, University of Tokyo, Hongo 7-3-1, Bunkyo-Ku, Tokyo, 113–8655, Japan

ARTICLE INFO

Article history:
Received 3 February 2011
Accepted 17 July 2011
Available online 23 July 2011

Keywords:
Auditory brainstem response
Cisplatin
Guinea pig
Hair cell
Polymeric micelle
Ototoxicity

ABSTRACT

Nanocarriers potentially reduce or prevent chemotherapy-induced side effects, facilitating the translation of nanocarrier formulation into the clinic. To date, organ-specific toxicity by nanocarriers remains to be clarified. Here, we studied the potential of polymeric micelle nanocarriers to prevent the ototoxicity, which is a common side effect of high-dose cisplatin (CDDP) therapy. In this study, we evaluated the ototoxicity of CDDP-incorporating polymeric micelles (NC-6004) in guinea pigs in comparison with that of cisplatin. Their auditory brainstem responses (ABRs) to 2, 6, 12, 20, and 30 kHz sound stimulation were measured before and 5 days after the drug administration. Groups treated with NC-6004 showed no apparent ABR threshold shifts, whereas groups treated with CDDP showed dose-dependent threshold shifts particularly at the higher frequencies. Consistent with the ABR results, groups treated with NC-6004 showed excellent hair-cell preservation, whereas groups treated with CDDP exhibited significant hair-cell loss ($P<0.05$). Synchrotron radiation-induced X-ray fluorescence spectrometry imaging demonstrated that the platinum distribution and concentration in the organ of Corti were significantly reduced ($P<0.01$) in guinea pigs treated with NC-6004 compared with guinea pigs treated with CDDP. These findings indicate that micellization of CDDP reduces its ototoxicity by circumventing the vulnerable cells in the inner ear.

1. Introduction

Recently, nanocarrier-mediated drug delivery has received great attention in cancer therapy since nanocarriers carrying chemotherapeutic agents have shown to enhance antitumor activity with reduced side effects [1–4]. The antitumor activity is enhanced because the tumor accumulation is augmented in the nanocarriers via the enhanced permeability and retention (EPR) effect [5], which is based on the following pathophysiological characteristics of solid tumors: hypervascularity, incomplete vascular architecture, secretion of vascular permeability factors stimulating extravasation within the cancer tissue, and the absence of effective lymphatic drainage. However, the reduction or prevention of chemotherapy-induced side effects, especially organ-specific toxicity, by nanocarriers remains to be completely clarified. The mechanisms of nanocarrier-mediated reduction of chemotherapy-induced organ-specific toxicity must be shown to facilitate the translation of nanocarrier formulation into the clinic.

Polymeric micelles, which are self-assemblies of block copolymers, have gained increasing popularity as nanocarriers for chemotherapeutic agents since their critical features, including size and drug loading and release, can be modulated by engineering block copolymers. Polymeric micelles carrying chemotherapeutic agents can selectively and effectively accumulate in the solid tumors, thereby leading to enhanced antitumor activity. Currently, our micelle formulations of paclitaxel (PTX), SN-38 (a biologically active metabolite of CPT-11), cisplatin (*cis*-dichlorodiammineplatinum(II), CDDP), and 1,2-diaminocyclohexane (DACHPt) are being tested in clinical trials. Regarding chemotherapy-induced side effects, polymeric micelles have been revealed to restrain the neurotoxicity of PTX and CDDP [6,7], intestinal toxicity of CPT-11 [8], and the nephrotoxicity of CDDP [7].

CDDP is a common chemotherapeutic agent used to treat many different types of cancer, including lung, gastrointestinal, bladder, and head and neck cancer. The major dose-limiting factors in CDDP therapy is the nephrotoxicity, which can be reversed to some extent by increasing the saline hydration and by using diuretic agents. As aforementioned, micellization of CDDP can prevent the nephrotoxicity,

* Corresponding author at: Department of Otolaryngology and Head and Neck Surgery, Graduate School of Medicine, University of Tokyo, Hongo 7-3-1, Bunkyo-ku, Tokyo 113–8655, Japan. Tel.: +81 3 5800 8924; fax: +81 3 3814 9486.
E-mail address: tyamasoba-tky@umin.ac.jp (T. Yamasoba).

0168-3659/$ – see front matter © 2011 Elsevier B.V. All rights reserved.
doi:10.1016/j.jconrel.2011.07.026

thereby allowing hydration-free CDDP treatment for the improvement of the patients' QOL.

CDDP-induced hearing loss is usually bilateral, irreversible, and cumulative. Audiological studies have indicated that up to 90% of the patients receiving CDDP experience significant hearing loss, especially at high frequencies [9]. The CDDP-induced hearing loss is particularly serious in pediatric populations because loss of hearing at this developmental stage hampers speech and cognitive and social development. Therefore, there is an imperative need for developing treatments that will ameliorate CDDP-induced ototoxicity. However, to date, no such cures or preventive treatments are available. In the present study, we evaluated the ototoxicity of polymeric micelles incorporating CDDP (NC-6004) in comparison with that of CDDP. NC-6004 has been evaluated in a phase I clinical trial in the United Kingdom [10], and the phase I/II trial is now underway in East Asia.

2. Materials and Methods

2.1. Materials

CDDP was purchased from WC Heraeus GmbH & Co., KG (Hanau, Germany). NC-6004 was prepared according to the slightly modified procedure that was previously reported [11] and supplied by NanoCarrier Co. Ltd. (Chiba, Japan). In brief, NC-6004 is a polymer–metal complex micelle comprising CDDP and sodium salt of poly (ethylene glycol)–poly(glutamic acid) block copolymer [PEG-P(Glu)] [11].

2.2. Animals

We used 20 healthy male Hartley-strain albino guinea pigs (weighing 243–314 g; Saitama Experimental Animals Supply Co. Ltd., Japan) with normal Preyer's reflex. The animals were housed, 5 together, in animal cages and given free access to food and water. A 12-hour dark-light cycle was maintained. They were anesthetized with a mixture of ketamine hydrochloride (40 mg/kg; Daiichi Sankyo Prophama Co. Ltd., Japan) and xylazine hydrochloride (10 mg/kg; Bayer Healthcare, Germany) during all measurements and intravenous injection procedures. All animal experiments conformed to the guidelines of the University Committee for the Use and Care of Animals, University of Tokyo, and the National Institutes of Health Guide for the Care and Use of Laboratory Animals.

2.3. Drug administration

The animals were divided into five groups according to the drug administered. Groups Cis(8) ($n=4$) and Cis(12) ($n=6$) received a bolus intravenous injection of 8 and 12 mg/kg CDDP, respectively, as well as 20 ml normal saline subcutaneously immediately after the injection to decrease the renal damage. Groups Cis-m(8) ($n=3$) and Cis-m(12) ($n=4$) received a bolus intravenous injection of NC-6004 comprising 8 and 12 mg/kg CDDP, respectively, but no subcutaneous hydration. The control group ($n=3$) received normal saline intravenously.

2.4. Auditory brainstem response measurement

Auditory brainstem responses (ABRs) were measured before and 5 days after the drug administration. The tympanic membranes were examined before the recording to ensure normal middle ear appearance. Needle electrodes were placed subcutaneously at the vertex (active electrode), beneath the pinna of the left ear (reference electrode), and beneath the right ear (ground electrode). The sound stimulus consisted of a 7 ms tone burst with a rise-fall time of 1 ms at 2, 6, 12, 20, and 30 kHz. The ABRs to 500 sweeps were averaged at each intensity level (5 dB steps) to assess the threshold, which was defined as the lowest intensity level at which a clear reproducible waveform is visible in the trace. When an ABR waveform could not be evoked, the threshold was assumed to be 5 dB greater than the maximum intensity produced by the system (105 dB sound pressure level). Threshold shifts were calculated by subtracting the pre-administration thresholds from the post-administration thresholds.

2.5. Hair-cell count

The animals in groups Cis(12) and Cis-m(12) were sacrificed under deep anesthesia after the ABR measurements and their left temporal bone was removed. The cochleae were harvested from the temporal bone and perfused with 4% paraformaldehyde in 0.1 M phosphate buffer (PFA) through a perforation in the apex and the opened oval window. They were postfixed in 4% PFA overnight and stored at 4 °C. PFA was removed by rinsing the samples in phosphate-buffered saline (PBS). The lateral wall, tectorial membrane, and Reissner's membrane were removed, and the cochlear sensory epithelium was detached from the bony shell. The epithelial cells were permeabilized in 0.3% Triton X-100 in PBS for 10 min, rinsed in PBS, stained with 1% rhodamine-phalloidin (Sigma Chemical Co., St. Louis, MO, USA) for 40 min, and once again rinsed in PBS. The organ of Corti was separated from the modiolus and mounted on glass slides. Surface preparation assessment was performed under confocal microscopy (LSM 510 META, Carl Zeiss, Inc., Jena, Germany). The total numbers of hair cells and damaged hair cells were counted from the apex to the basal turn. For the analysis of each cochlea, the whole length of the basilar membrane except the hook was assessed. A cytocochleogram was prepared by plotting the mean percentage of missing hair cells as a function of the percentage length of the organ of Corti.

2.6. Platinum distribution and concentration measurement

Synchrotron radiation-induced X-ray fluorescence spectrometry (μSR-XRF) imaging was performed to determine the platinum distribution in sections of the organ of Corti from groups Cis(12) and Cis-m(12). The left temporal bone was removed, surface preparation of the organ of Corti was performed as mentioned in the preceding, and the samples were fixed on polypropylene sheets. μSR-XRF was performed by using beam line 37XU at SPring-8 (Hyogo, Japan), at 8 GeV and about 100 mA. A photon beam with energy of 14 keV, a beam-spot size of $1.3\times1.3\ \mu m^2$, and intensity of 10^{12} photons/s was irradiated on the tissue samples. The fluorescence X-rays were measured by using a Si-SSD (Silicon solid state detector) in air at room temperature. The samples on the acryl board were then mounted on an x–y translation stage. The fluorescence X-ray intensity was normalized to the incident X-ray intensity, I_0, to produce a two-dimensional elemental map. Tissue sections of $250\times250\ \mu m^2$ were roughly scanned before the imaging. The count of platinum atoms in the samples was converted to the concentration of platinum by using the calibration standards (10 and 500 μM) of CDDP. The total intensity per tissue area was determined by using ImageJ 1.43u software (US National Institutes of Health).

2.7. Statistical analysis

We used SigmaStat software (Systat Software, Inc., Chicago, IL, USA) for statistical analysis. The ABR threshold shifts at each frequency were compared among the control and experimental groups. Bartlett's test was used to test the normality of the distribution, and one-way analysis of variance (ANOVA), Tukey–Kramer or Kruskal–Wallis test, or Dunn's test was used according to the distribution. The survival rates of the inner and outer hair cells in groups Cis(12) and Cis-m(12) were compared by using a two-tailed Student's t-test. A value of $P<0.05$ was considered statistically

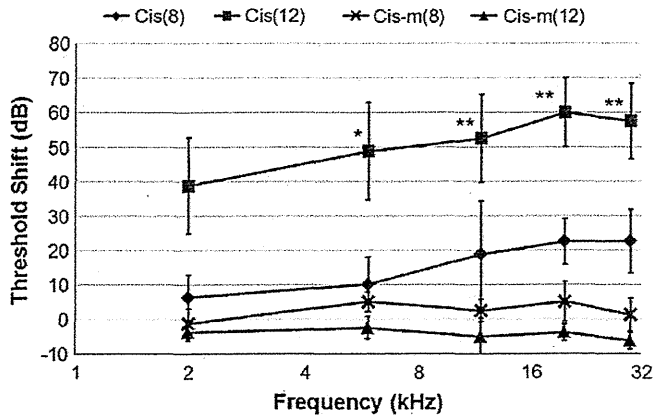

Fig. 1. ABR threshold shifts from the baseline to five days after drug administration. All results represent the mean ± SEM. *P<0.05, **P<0.01.

significant. The data were calculated as the mean ± standard error of the mean (SEM).

3. Results

Two animals in group Cis(12) died within four days of the 12 mg/kg CDDP administration (33% mortality), and were thus excluded from the data analysis. The LD_{50} for a single injection of CDDP is 9.7 mg/kg in guinea pigs [12].

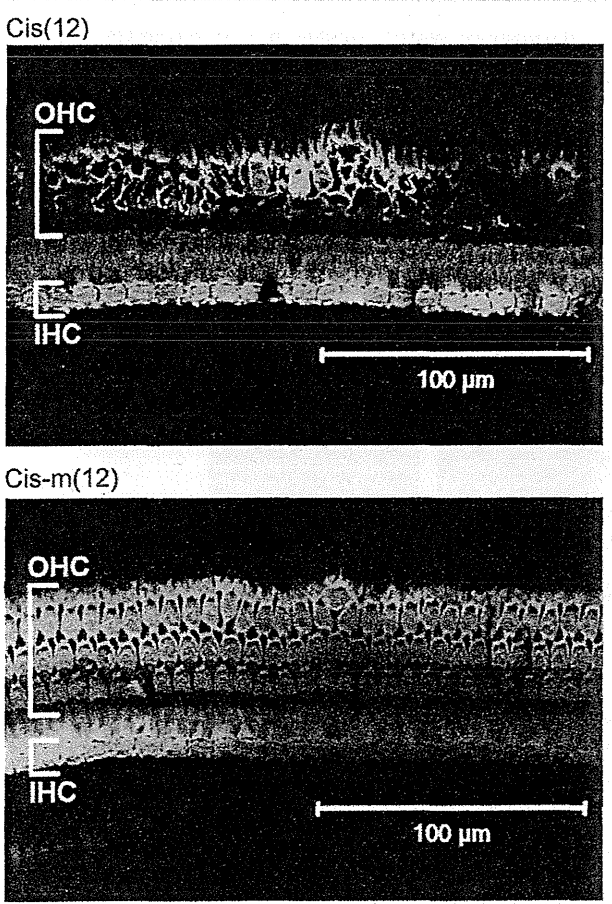

Fig. 2. Representative rhodamine-phalloidin-stained sections of the organ of Corti in the basal turn in groups Cis(12) (left) and Cis-m(12) (right). Three rows of the outer hair cells (OHCs) and a single row of the inner hair cells (IHCs) are well preserved in an animal treated with Cis-m(12), whereas almost all of the OHCs and a few IHCs are missing in an animal treated with Cis(12).

3.1. ABR threshold shifts

The ABR threshold shifts of the experimental groups are shown in Fig. 1. Group Cis(8) showed mild ABR threshold shifts (range = 6–23 dB) at the measured frequencies, but group Cis(12) demonstrated larger shifts (range = 39–60 dB) that were more severely affected by the higher frequencies. In contrast, groups Cis-m(8) and Cis-m(12) showed virtually no ABR threshold shifts. The Cis(8) ABR thresholds tended to be more affected than the Cis-m(8) ABR thresholds, although the differences between the groups were not statistically significant. Groups Cis(12) and Cis-m(12) had significant differences at all frequencies ($P<0.05$ at 2 kHz and $P<0.01$ at 6, 12, 20, and 30 kHz).

3.2. Hair-cell survival rates

In the normal organ of Corti, 3 rows of the outer hair cells (OHCs) and a single row of the inner hair cells (IHCs) can be observed. Fig. 2 shows the representative rhodamine-phalloidin-stained organ of Corti in the basal turn in groups Cis(12) and Cis-m(12). Significant damage of the OHCs and mild damage of the IHCs were observed in group Cis(12), whereas only few notable damages were observed in both the IHCs and OHCs in group Cis-m(12).

In terms of the IHC survival rates (Fig. 3A), approximately 10% of the IHCs were lost in group Cis(12) group, whereas less than 3% of these hair cells were lost in group Cis-m(12). Between the groups, significant differences in the IHC survival rate were noted at the distances of 30%, 40%, 70%, and 80% from the apex ($P<0.05$). The difference was also significant when the total IHC loss was compared ($P<0.05$).

Fig. 3B shows the survival rates of the OHCs in groups Cis(12) and Cis-m(12). Approximately 50% of these hair cells were lost in group Cis(12), whereas less than 15% were lost in group Cis-m(12). In group Cis(12), the extent of OHC loss ranged from 21% at 10% from the apex to 68% at 80% from the apex, indicating that the basal region was more severely affected than the apical region. Comparatively, the animals in group Cis-m(12) showed less damage in the OHCs, but similarly, the basal region was more severely affected than the apical region: the extent of OHC loss was less than 20% in all the segments except 90% from the apex (25% loss). These groups showed significant differences in the OHC survival rates at the distances of 20%, 40%, and 60–90% from the apex ($P<0.05$). The difference was also significant when the total OHC loss was compared ($P<0.05$).

3.3. Platinum distribution and concentration

Fig. 4 shows the platinum distribution in the organ of Corti in groups Cis(12) and Cis-m(12). Group Cis(12) had an apparently higher platinum concentration in the organ of Corti than group Cis-m(12). The mean intensity of platinum per tissue area of the organ of Corti (count/mm^2) was significantly greater in group Cis(12) than in group Cis-m(12) ($P<0.01$; Table 1).

4. Discussion

The main targets of CDDP in the cochlea are the OHCs in the organ of Corti and the stria vascularis, the vascularized epithelium in the cochlear lateral wall [13]. CDDP induces a caspase-dependent apoptotic pathway in these sensitive cochlear cells [14]. The molecular mechanisms that trigger apoptosis in the cochlea have not been elucidated, but several mechanisms have been proposed, such as increased generation of reactive oxygen species [13,15]. Platinum analogs, such as carboplatin [16] and oxaliplatin [17], have been developed to overcome the CDDP-related side effects. However, clinical trials have shown that the regimens including CDDP are still the most useful platinum-containing antineoplastic drugs [18]. Dozens of experimental studies have attempted to find ideal protective agents

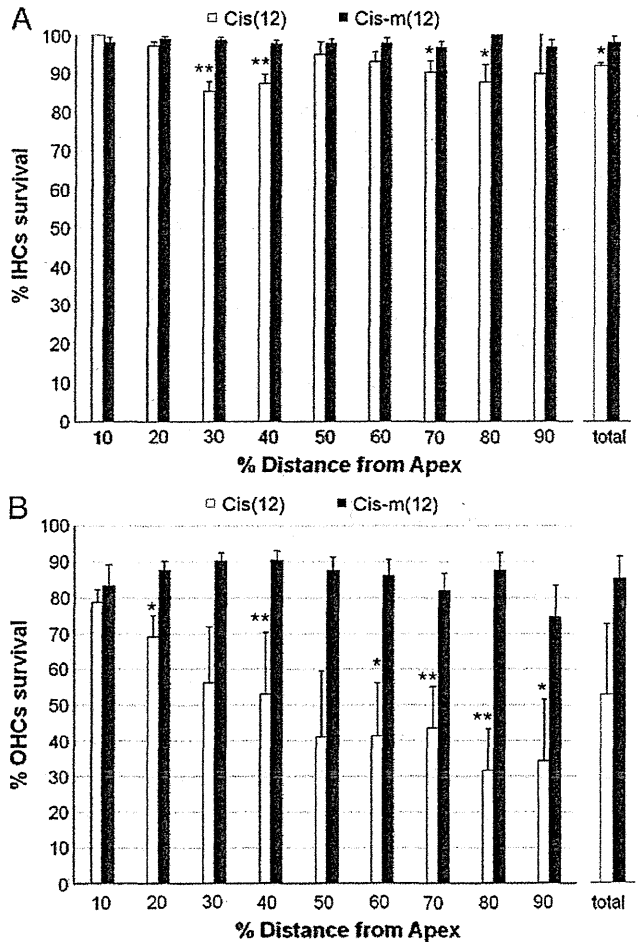

Fig. 3. Survival rates of the inner and outer hair cells in groups Cis(12) and Cis-m(12) determined five days after drug administration by using cytocochleograms. The survival rates of the inner (A) and outer (B) hair cells were calculated as percentages of the number of surviving hair cells in the experimental groups to that in the control group in each field. The results represent the mean ± SEM (n = 4 guinea pigs in each group). *P < 0.05, **P < 0.01.

against CDDP ototoxicity. Previous studies have shown that antioxidants, including sodium thiosulfate [19], D- or L-methionine [20,21], diethyldithiocarbamate [22,23], lipoic acid [24], and N-acetylcysteine [25], are useful in scavenging reactive oxygen species in the inner ear. However, systemic administration of L-methionine or sodium thiosulfate may inactive CDDP and reduces its antitumor activity. To prevent CDDP ototoxicity without reducing its antitumor activity, these agents require invasive approaches for delivery into the inner ear. Several other agents that protect from CDDP ototoxicity and also preserve its antitumor effect have been developed; round window application of adenosine A1 receptor agonists [26,27] and oral administration of ebselen and allopurinol [28], sodium butyrate [29], and salicylates [30] are partially effective in reducing CDDP ototoxicity without affecting its antitumor activity in animals. Until now, however, no clinical interventions have been shown to prevent CDDP ototoxicity and ensure safe therapy without reduced antitumor activity [31]. The development of a drug-delivery technology offering better selective accumulation of CDDP in solid tumors while lessening its distribution in normal tissues is therefore anticipated.

In this study, we evaluated the ototoxicity of NC-6004 and CDDP, and found that the animals given NC-6004 intravenously showed virtually no ABR threshold shifts, excellent inner and outer hair-cell preservation, and reduced platinum distribution and concentration in the organ of Corti compared with those that received the same doses of cisplatin. These results clearly indicate the markedly less-extensive ototoxicity of NC-6004.

The organ of Corti is isolated from the systemic circulation by the blood–cochlear barrier, which is similar to the blood–brain barrier [32]. CDDP readily penetrates this barrier and enters the perilymph of the inner ear, where it reaches the hair cells and exerts its toxic action. The limited cochlear uptake of oxaliplatin is considered responsible for the lower ototoxicity of oxaliplatin than CDDP [33]. The particle size of NC-6004 is approximately 30 nm [11] and that of the intrastrial space is approximately 15 nm [33,34]; therefore, the decreased ototoxicity of NC-6004 is mainly attributable to its circumvention of the IHCs and OHCs by not crossing the stria vascularis, which forms a part of the blood–cochlear barrier.

In the current study, the differences in the platinum distribution between animals treated with CDDP and NC-6004 were elucidated by

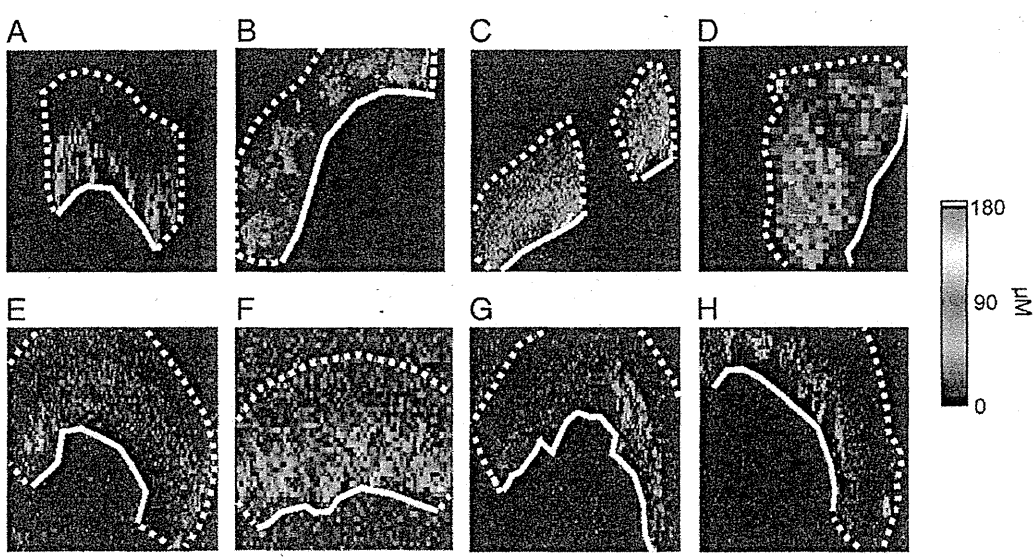

Fig. 4. Synchrotron radiation-induced X-ray fluorescence spectrometry images of the platinum distribution and concentration in the organ of Corti. The white lines indicate the basilar membrane and the areas surrounded by the broken lines indicate the presence of platinum. The cochlear epithelium in groups (A–D) Cis(12) and (E–H) Cis-m(12) at distances of approximately 20%, 40%, 60%, and 80% from the apex are shown.

Table 1
The mean intensity of platinum per tissue area (count/mm^2) shown in Fig. 4.

Group	Figure	Tissue area intensity	Background intensity	Tissue area-to-background intensity ratio
Cis(12)	A	22.06	3.39	6.51
Cis(12)	B	6.55	0.95	6.93
Cis(12)	C	21.99	3.85	5.72
Cis(12)	D	67.68	10.07	6.72
Average				6.47
Cis-m(12)	E	6.92	4.29	1.61
Cis-m(12)	F	48.81	33.63	1.45
Cis-m(12)	G	10.27	5.79	1.77
Cis-m(12)	H	8.92	5.39	1.65
Average				1.62

The data were rounded off to the second decimal place.

μSR-XRF. Until now, 2 sampling techniques have been used to measure the platinum concentration in the cochlea: sampling of the perilymph in the scala tympani [33] and homogenizing the cochlear tissue [35]. In either of the techniques, it is impossible to measure the platinum concentration only in the organ of Corti. In contrast, μSR-XRF enables (semi-)quantitative measurement of platinum concentration in the organ of Corti. The limitation of our technique is that its resolution is not high enough to distinguish each cell in the organ of Corti, which contains not only the hair cells but also the supporting cells. Thus, we could not measure the platinum concentration exclusively in the hair cells, one of the main targets of CDDP-induced cell damage. However, a previous immunohistochemical study [36], in which the CDDP was detected indirectly in the guinea pig cochlea by using an antiserum containing antibodies against CDDP-DNA adducts, showed that, while platinated DNA was present in the nuclei of most cells in the organ of Corti after CDDP administration, the nuclei of the OHCs exhibited prominent immunostaining, with the nuclei of all other (supporting) cells being only weakly stained. Therefore, it is reasonable that the platinum concentration in the organ of Corti measured by μSR-XRF is mainly derived from the OHCs.

Reportedly, there is a large difference in the CDDP concentration between the perilymph and the blood, and ABR threshold shifts are related to the CDDP concentration in the blood but not in the perilymph [37]. These findings suggest that a high plasma concentration of CDDP could collapse the blood–cochlear barrier at the initial stage after CDDP administration. NC-6004 is a long-circulating carrier with a gradual-release profile of CDDP [11]. Therefore, the reduced ototoxicity of NC-6004 can also be explained by the possibility that the gradual-release profile of CDDP from NC-6004 avoids an abrupt transient increase in the plasma CDDP concentration at the initial stage after its administration, thereby preserving the blood–cochlear barrier. This view is consistent with the fact that NC-6004 has negligible nephrotoxicity compared with CDDP, which shows a transient increase in its initial blood concentration [7]. There is also a significant correlation between the plasma creatinine level, an indicator of renal function, and the concentration of platinum [38]. Therefore, the reduced nephrotoxicity of NC-6004 might contribute to its reduced ototoxicity.

5. Conclusion

The present study demonstrated that the systemic administration of CDDP induced dose-dependent ABR threshold shifts and hair cell damage in guinea pigs, whereas such adverse effects were virtually absent after the systemic administration of NC-6004. The μSR-XRF imaging showed that the platinum distribution in the organ of Corti was significantly reduced by the micellization of CDDP. These findings confirm that the micellization of CDDP reduces its ototoxicity without additional administration of protective agents, and these findings have not been reported in previous studies. This advantage will improve patient compliance in cancer chemotherapy while maintaining substantial antitumor efficacy.

Acknowledgements

This research was supported by the Funding Program for World-Leading Innovative R&D on Science and Technology (FIRST Program) of the Japan Society for the Promotion of Science (JSPS) (to K.K.), the Core Research Program for Evolutional Science and Technology (CREST) of the Japan Science and Technology Corporation (JST) (to K.K.), and Grants-in-Aid for Scientific Research from the Japanese Ministry of Education, Culture, Sports, Science and Technology (to Y.M. and T.Y.).

References

[1] P.A. Vasey, S.B. Kaye, R. Morrison, C. Twelves, P. Wilson, R. Duncan, A.H. Thomson, L.S. Murray, T.E. Hilditch, T. Murray, S. Burtles, D. Fraier, E. Frigerio, J. Cassidy, Phase I clinical and pharmacokinetic study of PK1 [N-(2-hydroxypropyl) methacrylamide copolymer doxorubicin]: first member of a new class of chemotherapeutic agents-drug-polymer conjugates. Cancer Research Campaign Phase I/II Committee, Clin. Cancer Res. 5 (1999) 83–94.
[2] T. Lian, R.J. Ho, Trends and developments in liposome drug delivery systems, J. Pharm. Sci. 90 (2001) 667–680.
[3] M.E. Davis, Z.G. Chen, D.M. Shin, Nanoparticle therapeutics: an emerging treatment modality for cancer, Nat. Rev. Drug Discov. 7 (2008) 771–782.
[4] M. Orditura, F. Quaglia, F. Morgillo, E. Martinelli, E. Lieto, G. De Rosa, D. Comunale, M.R. Diadema, F. Ciardiello, G. Catalano, F. De Vita, Pegylated liposomal doxorubicin: pharmacologic and clinical evidence of potent antitumor activity with reduced anthracycline-induced cardiotoxicity (review), Oncol. Rep. 12 (2004) 549–556.
[5] Y. Matsumura, H. Maeda, A new concept for macromolecular therapeutics in cancer chemotherapy: mechanism of tumoritropic accumulation of proteins and the antitumor agent smancs, Cancer Res. 46 (1986) 6387–6392.
[6] T. Hamaguchi, Y. Matsumura, M. Suzuki, K. Shimizu, R. Goda, I. Nakamura, I. Nakatomi, M. Yokoyama, K. Kataoka, T. Kakizoe, NK105, a paclitaxel-incorporating micellar nanoparticle formulation, can extend in vivo antitumour activity and reduce the neurotoxicity of paclitaxel, Br. J. Cancer 92 (2005) 1240–1246.
[7] H. Uchino, Y. Matsumura, T. Negishi, F. Koizumi, T. Hayashi, T. Honda, N. Nishiyama, K. Kataoka, S. Naito, T. Kakizoe, Cisplatin-incorporating polymeric micelles (NC-6004) can reduce nephrotoxicity and neurotoxicity of cisplatin in rats, Br. J. Cancer 93 (2005) 678–687.
[8] Y. Matsumura, Preclinical and clinical studies of NK012, an SN-38-incorporating polymeric micelles, which is designed based on EPR effect, Adv. Drug Deliv. Rev. 63 (2011) 184–192.
[9] L. Helson, E. Okonkwo, L. Anton, E. Cvitkovic, cis-Platinum ototoxicity, Clin. Toxicol. 13 (1978) 469–478.
[10] R. Plummer, R.H. Wilson, H. Calvert, A.V. Boddy, M. Griffin, J. Sludden, M.J. Tilby, M. Eatock, D.G. Pearson, C.J. Ottley, Y. Matsumura, K. Kataoka, T. Nishiya, A Phase I clinical study of cisplatin-incorporated polymeric micelles (NC-6004) in patients with solid tumours, Br. J. Cancer 104 (2011) 593–598.
[11] N. Nishiyama, S. Okazaki, H. Cabral, M. Miyamoto, Y. Kato, Y. Sugiyama, K. Nishio, Y. Matsumura, K. Kataoka, Novel cisplatin-incorporated polymeric micelles can eradicate solid tumors in mice, Cancer Res. 63 (2003) 8977–8983.
[12] R.W. Fleischman, S.W. Stadnicki, M.F. Ethier, U. Schaeppi, Ototoxicity of cis-dichlorodiammine platinum (II) in the guinea pig, Toxicol. Appl. Pharmacol. 33 (1975) 320–332.
[13] L.P. Rybak, C.A. Whitworth, D. Mukherjea, V. Ramkumar, Mechanisms of cisplatin-induced ototoxicity and prevention, Hear. Res. 226 (2007) 157–167.
[14] A. Forge, L. Li, Apoptotic death of hair cells in mammalian vestibular sensory epithelia, Hear. Res. 139 (2000) 97–115.
[15] N. Dehne, J. Lautermann, F. Petrat, U. Rauen, H. de Groot, Cisplatin ototoxicity: involvement of iron and enhanced formation of superoxide anion radicals, Toxicol. Appl. Pharmacol. 174 (2001) 27–34.
[16] M. Wake, S. Takeno, D. Ibrahim, R. Harrison, Selective inner hair cell ototoxicity induced by carboplatin, Laryngoscope 104 (1994) 488–493.
[17] C.A. Rabik, M.E. Dolan, Molecular mechanisms of resistance and toxicity associated with platinating agents, Cancer Treat. Rev. 33 (2007) 9–23.
[18] J. Lokich, What is the "best" platinum: cisplatin, carboplatin, or oxaliplatin? Cancer Invest. 19 (2001) 756–760.
[19] W.C. Otto, R.D. Brown, L. Gage-White, S. Kupetz, M. Anniko, J.E. Penny, C.M. Henley, Effects of cisplatin and thiosulfate upon auditory brainstem responses of guinea pigs, Hear. Res. 35 (1988) 79–85.
[20] K.C. Campbell, L.P. Rybak, R.P. Meech, L. Hughes, D-methionine provides excellent protection from cisplatin ototoxicity in the rat, Hear. Res. 102 (1996) 90–98.
[21] D. Reser, M. Rho, D. Dewan, L. Herbst, G. Li, H. Stupak, K. Zur, J. Romaine, D. Frenz, L. Goldbloom, R. Kopke, J. Arezzo, T. Van De Water, L- and D-methionine provide equivalent long term protection against CDDP-induced ototoxicity in vivo, with partial in vitro and in vivo retention of antineoplastic activity, Neurotoxicology 20 (1999) 731–748.
[22] M.W. Church, J.A. Kaltenbach, B.W. Blakley, D.L. Burgio, The comparative effects of sodium thiosulfate, diethyldithiocarbamate, fosfomycin and WR-2721 on ameliorating cisplatin-induced ototoxicity, Hear. Res. 86 (1995) 195–203.

[23] L.P. Rybak, K. Husain, C. Morris, C. Whitworth, S. Somani, Effect of protective agents against cisplatin ototoxicity, Am. J. Otol. 21 (2000) 513–520.
[24] L.P. Rybak, K. Husain, C. Whitworth, S.M. Somani, Dose dependent protection by lipoic acid against cisplatin-induced ototoxicity in rats: antioxidant defense system, Toxicol. Sci. 47 (1999) 195–202.
[25] D. Thomas Dickey, L.L. Muldoon, D.F. Kraemer, E.A. Neuwelt, Protection against cisplatin-induced ototoxicity by N-acetylcysteine in a rat model, Hear. Res. 193 (2004) 25–30.
[26] M.S. Ford, S.B. Maggirwar, L.P. Rybak, C. Whitworth, V. Ramkumar, Expression and function of adenosine receptors in the chinchilla cochlea, Hear. Res. 105 (1997) 130–140.
[27] C.A. Whitworth, V. Ramkumar, B. Jones, N. Tsukasaki, L.P. Rybak, Protection against cisplatin ototoxicity by adenosine agonists, Biochem. Pharmacol. 67 (2004) 1801–1807.
[28] E.D. Lynch, R. Gu, C. Pierce, J. Kil, Combined oral delivery of ebselen and allopurinol reduces multiple cisplatin toxicities in rat breast and ovarian cancer models while enhancing anti-tumor activity, Anticancer Drugs 16 (2005) 569–579.
[29] M. Drottar, M.C. Liberman, R.R. Ratan, D.W. Roberson, The histone deacetylase inhibitor sodium butyrate protects against cisplatin-induced hearing loss in guinea pigs, Laryngoscope 116 (2006) 292–296.
[30] G. Li, S.H. Sha, E. Zotova, J. Arezzo, T. Van de Water, J. Schacht, Salicylate protects hearing and kidney function from cisplatin toxicity without compromising its oncolytic action, Lab Invest. 82 (2002) 585–596.
[31] G.W. Hill, D.K. Morest, K. Parham, Cisplatin-induced ototoxicity: effect of intratympanic dexamethasone injections, Otol. Neurotol. 29 (2008) 1005–1011.
[32] V. Hellberg, I. Wallin, S. Eriksson, E. Hernlund, E. Jerremalm, M. Berndtsson, S. Eksborg, E.S. Arnér, M. Shoshan, H. Ehrsson, G. Laurell, Cisplatin and oxaliplatin toxicity: importance of cochlear kinetics as a determinant for ototoxicity, J. Natl. Cancer Inst. 101 (2009) 37–47.
[33] S.S. Spicer, B.A. Schulte, Novel structures in marginal and intermediate cells presumably relate to functions of apical versus basal strial strata, Hear. Res. 200 (2005) 87–101.
[34] H. Hibino, Y. Kurachi, Molecular and physiological bases of the K+ circulation in the mammalian inner ear, Physiology (Bethesda) 21 (2006) 336–345.
[35] R. Ramírez-Camacho, D.E. Fernández, J.M. Verdaguer, M.M. Gómez, A. Trinidad, J.R. García-Berrocal, M.A. Corvillo, Cisplatin-induced hearing loss does not correlate with intracellular platinum concentration, Acta Otolaryngol. 128 (2008) 505–509.
[36] M.W. van Ruijven, J.C. de Groot, F. Hendriksen, G.F. Smoorenburg, Immunohistochemical detection of platinated DNA in the cochlea of cisplatin-treated guinea pigs, Hear. Res. 203 (2005) 112–121.
[37] J.W. Sepmeijer, S.F. Klis, Distribution of platinum in blood and perilymph in relation to cisplatin induced ototoxicity in the guinea pig, Hear. Res. 247 (2009) 34–39.
[38] C. Lanvers-Kaminsky, B. Krefeld, A.G. Dinnesen, D. Deuster, E. Seifert, G. Würthwein, U. Jaehde, A.C. Pieck, J. Boos, Continuous or repeated prolonged cisplatin infusions in children: a prospective study on ototoxicity, platinum concentrations, and standard serum parameters, Pediatr. Blood Cancer 47 (2006) 183–193.

Journal of Controlled Release 151 (2011) 104–109

Contents lists available at ScienceDirect

Journal of Controlled Release

journal homepage: www.elsevier.com/locate/jconrel

Concept Paper

In situ quantitative monitoring of polyplexes and polyplex micelles in the blood circulation using intravital real-time confocal laser scanning microscopy

Takahiro Nomoto [a,1], Yu Matsumoto [b,c,d,1], Kanjiro Miyata [b], Makoto Oba [e], Shigeto Fukushima [f], Nobuhiro Nishiyama [b], Tatsuya Yamasoba [c], Kazunori Kataoka [a,b,f,*]

[a] Department of Bioengineering, Graduate School of Engineering, The University of Tokyo, Japan
[b] Division of Clinical Biotechnology, Center for Disease Biology and Integrative Medicine, Graduate School of Medicine, The University of Tokyo, Japan
[c] Department of Otorhinolaryngology and Head and Neck Surgery, Graduate School of Medicine and Faculty of Medicine, The University of Tokyo, Japan
[d] Department of Otorhinolaryngology and Head and Neck Surgery, Mitsui Memorial Hospital, Japan
[e] Department of Vascular Regeneration, Division of Tissue Engineering, The University of Tokyo Hospital, Japan
[f] Department of Materials Engineering, Graduate School of Engineering, The University of Tokyo, Japan

ARTICLE INFO

Article history:
Received 12 January 2011
Accepted 10 February 2011
Available online 3 March 2011

Keywords:
Intravital confocal microscopy
Polyplex
Polyethylene glycol
Block copolymer
Polymer micelle

ABSTRACT

Surface modification using poly(ethylene glycol) (PEG) is a widely used strategy to improve the biocompatibility of cationic polymer-based nonviral gene vectors (polyplexes). A novel method based on intravital real-time confocal laser scanning microscopy (IVRTCLSM) was applied to quantify the dynamic states of polyplexes in the bloodstream, thereby demonstrating the efficacy of PEGylation to prevent their agglomeration. Blood flow in the earlobe blood vessels of experimental animals was monitored in a noninvasive manner to directly observe polyplexes in the circulation. Polyplexes formed distinct aggregates immediately after intravenous injection, followed by interaction with platelets. To quantify aggregate formation and platelet interaction, the coefficient of variation and Pearson's correlation coefficient were adopted. In contrast, polyplex micelles prepared through self-assembly of plasmid DNA with PEG-based block catiomers had dense PEG palisades, revealing no formation of aggregates without visible interaction with platelets during circulation. This is the first report of *in situ* monitoring and quantification of the availability of PEGylation to prevent polyplexes from agglomeration over time in the blood circulation. This shows the high utility of IVRTCLSM in drug and gene delivery research.

1. Concept of new methodologies

Gene therapy offers a unique potential for the treatment of genetic and intractable diseases and for tissue engineering. Its success is dependent upon the development of useful gene vectors as well as application of a drug delivery system (DDS). Nonviral gene vectors are attractive alternatives to viral gene vectors because they are much simpler to produce, transport and store, and induce fewer immune responses. Cationic polymers that electrostatically interact with plasmid DNA (pDNA) have been widely studied as materials to construct nonviral gene vectors [1–5]. The cationic polymers most commonly used as gene vectors include branched polyethylenimine (BPEI), linear polyethylenimine, poly(L-lysine) (PLys), chitosan, and dendrimers [6]. These polymers form polyion complexes (polyplexes) with pDNA to successfully transfer it into cultured cells to induce appreciable level of gene expression. However, these polyplexes have biocompatibility problems for systemic application. Polyplexes usually require excess polycations to generate electrostatic repulsion for their increased solubility and colloidal stability. This eventually results in a shift of their surface charge to a positive value. This positive charge causes nonspecific interaction with anionic components in the body such as plasma proteins and blood cells, which might lead to severe adverse effects [7,8]. Attachment of hydrophilic polymers such as poly(ethylene glycol) (PEG) is called "PEGylation" and has often been used to shield nonviral gene vectors from undesired interaction in the blood. PEGylation also contributes to diminished uptake by the reticuloendothelial system or macrophages, and hence the half-life in blood circulation can be extended.

It is well documented that a PEG palisade prevents nonspecific interaction with biological components. However, *in situ* evaluation of

Abbreviations: PEG, poly(ethylene glycol); DDS, drug delivery system; pDNA, plasmid DNA; BPEI, branched polyethylenimine; PLys, poly(L-lysine); PEG-PLys, poly(ethylene glycol)-*b*-poly(L-lysine); PAsp(DET), poly[*N*-[*N*-(2-aminoethyl)-2-aminoethyl]aspartamide]; PEG-PAsp(DET), poly(ethylene glycol)-*b*-poly[*N*-[*N*-(2-aminoethyl)-2-aminoethyl] aspartamide]; IVRTCLSM, intravital real-time confocal laser scanning microscopy; CV, coefficient of variation; PCC, Pearson's correlation coefficient.

* Corresponding author at: Department of Materials Engineering, Graduate School of Engineering, The University of Tokyo, 7-3-1 Hongo, Bunkyo-ku, Tokyo 113-0033, Japan. Tel.: +81 3 5841 7138; fax: +81 3 5841 7139.
E-mail address: kataoka@bmw.t.u-tokyo.ac.jp (K. Kataoka).
[1] These authors equally contributed to this work.

0168-3659/$ – see front matter © 2011 Elsevier B.V. All rights reserved.
doi:10.1016/j.jconrel.2011.02.011

the interaction between nonviral gene vectors and biological components has not been reported due to the absence of methodology to quantify the interaction. We recently described a method of direct and instantaneous observation of intravenously injected substances using intravital real-time confocal laser scanning microscopy (IVRTCLSM) [9]. IVRTCLSM provides high-speed scanning and simultaneous capture of multicolor fluorescence. The macromolecular agents flowing in the bloodstream in tumors, kidneys, and livers can be monitored using IVRTCLSM.

In the present study, we applied IVRTCLSM for the investigation of the interaction between nonviral gene vectors and biological components *in situ*. For the PEGylated polyplexes, we focused on polyplex micelles made through the self-assembly of pDNA with PEG-based cationic block copolymers [10–12]. We further developed an analytical methodology to quantify the dynamic states of nonviral gene vectors circulating in the bloodstream. This is the first report visualizing and quantifying the interaction between nonviral gene vectors and biological components over time and in real-time *in situ*.

2. Experimental methods

2.1. Sample preparation

Sterile Hepes (1 M, pH 7.3) was purchased from Amresco (Solon, OH, USA) and used as a buffer solution after dilution with distilled water. pDNA encoding the soluble form of vascular endothelial growth factor receptor-1 was labeled with Cy5 using Label IT Tracker Nucleic Acid Localization Kits (Mirus Bio Corporation, Madison, WI, USA). BPEI (molecular weight (MW) 22 kDa; Sigma-Aldrich, St. Louis, MO, USA) was dialyzed in 0.01 M HCl and lyophilized as a hydrochloride salt. BPEI and PLys (hydrobromide salt, MW 4–15 kDa; Sigma-Aldrich) were mixed with Cy5-labeled pDNA (150 μg/mL) at an N/P ratio of 6 and 2, respectively, to form polyplexes. The N/P ratio was defined as the residual molar ratio of amino groups of cationic segment to phosphate groups of pDNA. Poly {*N*-[*N*-(2-aminoethyl)-2-aminoethyl]aspartamide} (PAsp(DET)) (polymerization degree: 95) was synthesized as described previously [13]. PAsp(DET) was mixed with Cy5-labeled pDNA at an N/P ratio of 4. Poly(ethylene glycol)-*b*-poly(L-lysine) (PEG-PLys; MW of PEG: 12,000; polymerization degree of PLys segment: 45) was synthesized as described previously [14]. Poly(ethylene glycol)-*b*-poly{*N*-[*N*-(2-aminoethyl)-2-aminoethyl]aspartamide} (PEG-PAsp(DET); MW of PEG: 12,000 Da; polymerization degree of PAsp(DET) segment: 93) was synthesized by the aminolysis of PEG-poly(β-benzyl L-aspartate) block copolymer with diethylenetriamine according to a previous report [13]. PEG-PLys/pDNA and PEG-PAsp(DET)/pDNA micelles were prepared at an N/P ratio of 2 and 4, respectively. The final Cy5-labeled pDNA concentration was adjusted to 100 μg/mL in 10 mM Hepes buffer (pH 7.3).

2.2. Animal preparation

All animal experimental procedures were executed in accordance with the Guide for the Care and Use of Laboratory Animals as stated by the National Institutes of Health. Balb/c nude mice (female; Charles River Laboratories, Tokyo, Japan) were anesthetized with 3.0%–4.0% isoflurane (Abbott Japan Co., Ltd., Tokyo, Japan) using a Univenter 400 Anaesthesia Unit (Univentor Ltd., Zejtun, Malta). Mice were then subjected to lateral tail vein catheterization with a 30-gauge needle (Dentronics Co., Ltd., Tokyo, Japan) connected to a nontoxic, medical grade polyethylene tube (Natsume Seisakusho Co., Ltd., Tokyo, Japan). Platelets were labeled *in vivo* with the intravenous injection of DyLight 488-conjugated anti-GPIbβ antibody (X488; EMFRET Analytics, Eibelstadt, Germany) following the manufacturer's instructions. Mice were placed onto a custom-designed temperature-controlled microscope stage. The ear lobe was attached beneath the cover slip with a single drop of immersion oil as described in our previous report [9]. Video acquisition of the dermis tissue at a speed of 30 frames per second was performed for 10 min. Two-hundred microliters of naked pDNA, polyplexes, and micelles (20 μg of pDNA) were administered via the tail vein catheter 10 s after video acquisition was initiated. For the platelet inhibition study, 300 μL of aspirin (acetylsalicylic acid; Sigma-Aldrich) saturated aqueous solution was orally administered to mice for 2 consecutive days before IVRTCLSM.

2.3. IVRTCLSM imaging and processing

All picture/movie acquisitions were performed using a Nikon A1R confocal laser scanning microscope system attached to an upright ECLIPSE FN1 machine equipped with a CFI Apo 40× WI λS objective lens (Nikon, Tokyo, Japan). All pictures/movies were acquired at a scale of 79.55 μm × 79.55 μm with 5.11 μm of confocal slice. Acquired data were further processed using Nikon NIS Elements software. The region of interest (ROI) was manually defined in the vein. Image frames were extracted every 5 s from the video data for further analyses. For quantification of aggregates, the coefficient of variation (*CV*) of Cy5 fluorescence was calculated. For the platelet interaction study, colocalization between DyLight and Cy5 was evaluated by Pearson's correlation coefficient (PCC) [15]. All obtained values were plotted against time.

3. Discovery

3.1. Real-time observation of aggregates

We prepared BPEI/pDNA (N/P = 6), PLys/pDNA (N/P = 2), and PAsp (DET)/pDNA (N/P = 4) polyplexes as well as PEG-PLys/pDNA (N/P = 2) and PEG-PAsp(DET)/pDNA (N/P = 4) micelles. BPEI/pDNA was used as the representative polyplex containing excessive polycations. N/P ratios of PLys/pDNA and PAsp(DET)/pDNA were determined as the critical ratio to condense pDNA according to our previous report [16]. N/P ratios of PEG-PLys/pDNA and PEG-PAsp(DET)/pDNA micelles were determined at the same N/P ratios of PLys/pDNA and PAsp(DET)/pDNA polyplexes, respectively. The size and zeta potentials of these polyplexes and polyplex micelles were summarized in Supplementary Table 1.

Intravenously injected polyplexes and micelles were directly observed by IVRTCLSM. These dynamic states in the bloodstream were compared (Supplementary Videos 1–5). Extracted movie frames at indicated time points are shown in Fig. 1. Immediately after the BPEI/pDNA polyplex was injected, the fluorescence of Cy5 agglomerated into clumps with a variable size in several micrometers range. This nonuniform fluorescence distribution of the polyplex indicated formation of aggregates. PLys/pDNA and PAsp(DET)/pDNA polyplexes showed similar aggregate formation. In contrast, the fluorescence of Cy5 showed uniform distribution when PEG-PLys/pDNA and PEG-PAsp(DET)/pDNA micelles were injected, indicating the absence of aggregates.

3.2. Quantification of aggregates

Using the mean intensity of Cy5 fluorescence, the amount of Cy5-labeled pDNA was evaluated. We acquired the images every 5 s, calculated the relative fluorescence intensity defined as (Cy5 mean fluorescence intensity - Cy5 minimum fluorescence intensity)/(Cy5 maximum fluorescence intensity − Cy5 minimum fluorescence intensity), and plotted the relative fluorescence intensities against time. (Supplementary Fig. 1) The relative fluorescence intensities of naked pDNA decreased immediately, and almost disappeared within 5 min after the start of acquisition. The relative fluorescence intensities of BPEI/pDNA, PLys/pDNA, and PAsp(DET)/pDNA polyplexes also rapidly decreased and dropped to around 0.2 within 10 min after the start of acquisition. In contrast, PEG-PLys/pDNA, and PEG-PAsp(DET)/pDNA polyplex micelles maintained the relative

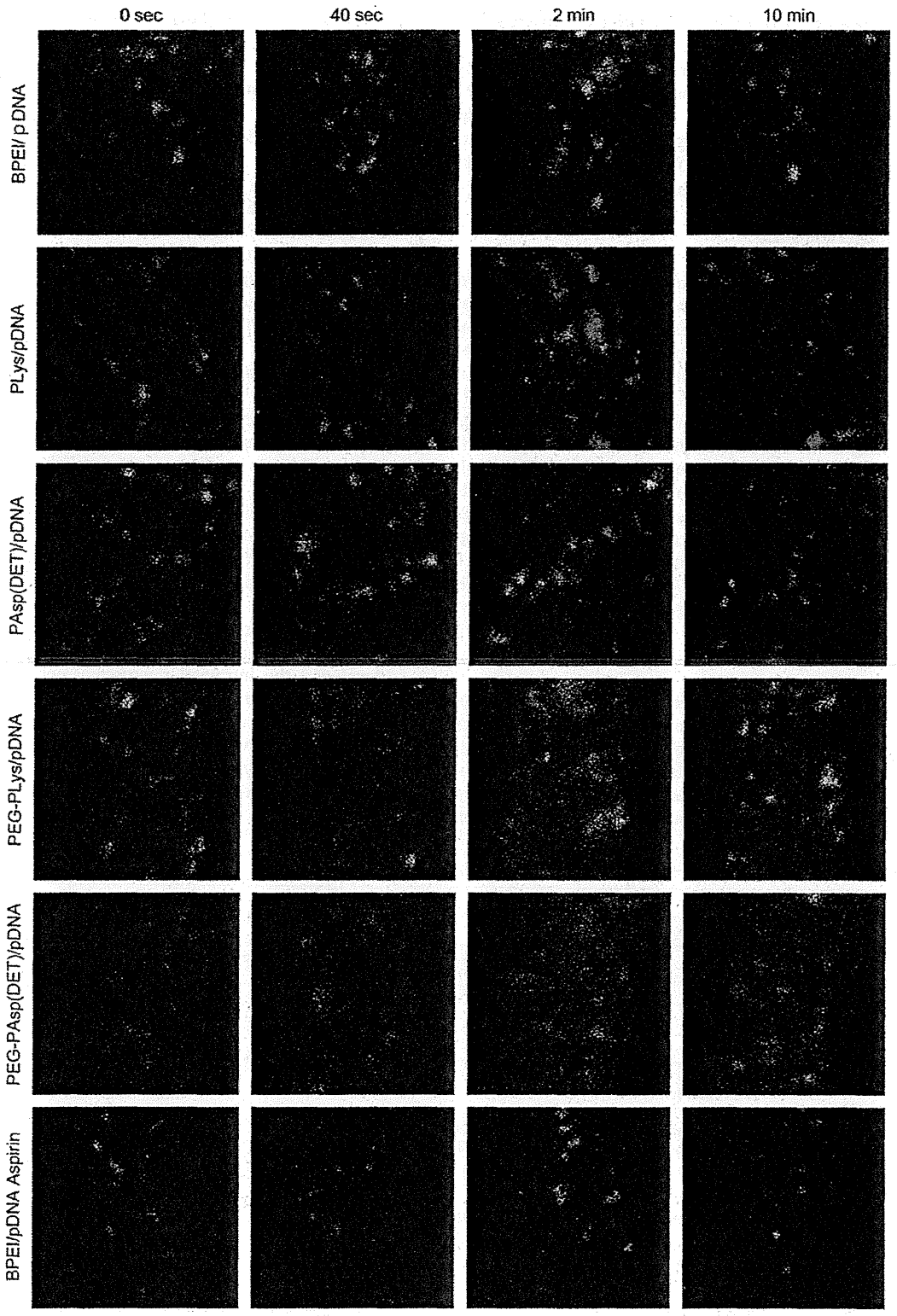

Fig. 1. Intravital confocal micro-videography of polyplexes and polyplex micelles in the bloodstream of the mouse earlobe. Prior to observation, the anti-GPIbβ antibody conjugated with DyLight 488 was injected to label platelets (green). The polyplexes and polyplex micelles incorporating Cy5-labeled pDNA (red) were intravenously injected 10 s after start of observation. Image frames were extracted from videos at identical time points for comparison. Image size: 79.55 μm × 79.55 μm. Confocal slice: 5.11 μm.

fluorescence intensities of around 0.9 and 0.7 even 10 min after the start of acquisition, suggesting the prolonged blood circulation. These results are consistent with the previous studies, which demonstrated pDNA degradation within 5 min and the improvement of blood circulation by PEGylation [17,18].

However, the relative fluorescence intensities could not provide the information about the aggregates of polyplexes and polyplex micelles. Thus, the quantification of aggregates was performed by CV calculation of Cy5 fluorescence in the ROI. The CV is a normalized measure of dispersion of a distribution, and is defined as the ratio of

the standard deviation to the mean. We acquired the images every 5 s, calculated the CV, and plotted the CV against time (Fig. 2). CV values of the polyplexes rapidly increased upon first entry into the vein of the earlobe immediately after intravenous injection. CV values of the polyplexes subsequently fluctuated and decreased over time. In contrast, CV values of the micelles slightly increased upon first entry due to the admixture of micelles and blood, and remained at a plateau at the lower values without fluctuation.

3.3. Platelet interaction study

Platelet is known to be the primary cell components involved in the initial event of thrombosis, and polycations initiate the process of platelet clots formation [19–21]. Thus, in this study, we focused on platelets interaction with cationic polyplexes. To investigate the interaction of polyplexes with platelets, we labeled platelets with DyLight 488-conjugated anti-GPIbβ antibody, and observed the interaction using IVRTCLSM (Fig. 1, Supplementary Videos 1–5). The average labeling efficiency of the antibody has been reported to be ~90% [22]. BPEI/pDNA, PLys/pDNA, and PAsp(DET)/pDNA polyplexes formed aggregates immediately after injection as described above. Their adhesion to platelets was clearly observed approximately 2 min after injection as judged from the colocalization of red and green fluorescences to appear as yellow colored pixels. In contrast, PEG-PLys/pDNA and PEG-PAsp(DET)/pDNA micelles showed no adhesion to platelets throughout the whole experiment.

3.4. Platelet interaction quantification

To quantify the interaction between polyplexes and platelets, we acquired the images every 5 s, and calculated the colocalization between Cy5 fluorescence and DyLight 488 fluorescence using PCC [15]. PCC indicates the intensity of the correlation of two elements, ranging from −1 to +1. The PCC value of the BPEI/pDNA polyplex fluctuated and increased up to approximately 0.4 (Fig. 3). PLys/pDNA and PAsp(DET)/pDNA polyplexes also fluctuated and increased up to approximately 0.25 and 0.33, respectively. In contrast, PCC values of PEG-PLys/pDNA and PEG-PAsp(DET)/pDNA micelles were maintained at almost zero throughout the study.

3.5. Platelet inhibition study

To investigate whether inhibition of platelet function decreases aggregates formation, aspirin was used as an anti-platelet agent. We compared the CV and PCC of the BPEI/pDNA polyplex between aspirin-administered mice and nonadministered control mice (Figs. 1 and 4, Supplementary Video 6). The CV value of the aspirin-administered mice was almost identical to that of control mice; however, their PCC value remained <0.1 throughout the study.

4. Interpretation and significance of new methodologies

Pharmacokinetic studies are indispensable for developing efficient DDSs that transport drugs specifically to the targeted tissue. Pharmacokinetic studies using animals have primarily relied on *ex vivo* techniques, such as analyzing blood or urine samples. These *ex vivo* techniques have been well established to analyze blood circulation, target accumulation, or other pharmacological information of the DDS. However, this approach provides only static information at specific time points. Therefore, investigating dynamic and longitudinal events using this approach is difficult. Alternatively, the intravital microscopy is an emerging technique [23], allowing to investigate such dynamic states of DDS in animals. Recently, we developed the intravital microscopy equipped with fast-scanning laser confocal systems (IVRTCLSM) [9], and demonstrated here its application as a novel tool to dynamically evaluate the interaction between gene vectors and blood components. Our method is characterized by noninvasive observation with high spatial and temporal resolutions to quantitatively monitor the dynamic states

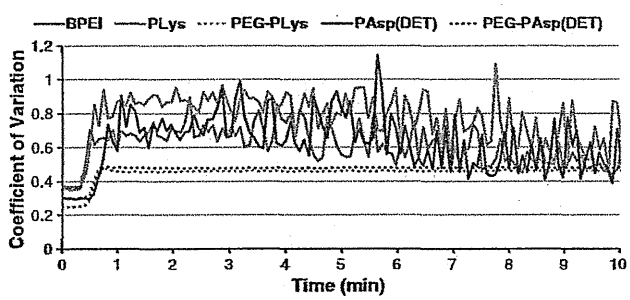

Fig. 2. Quantification of aggregates of polyplexes and micelles. Aggregates of polyplexes and micelles were quantified with CV of Cy5 fluorescence intensities in the frames extracted every 5 s from crude videos.

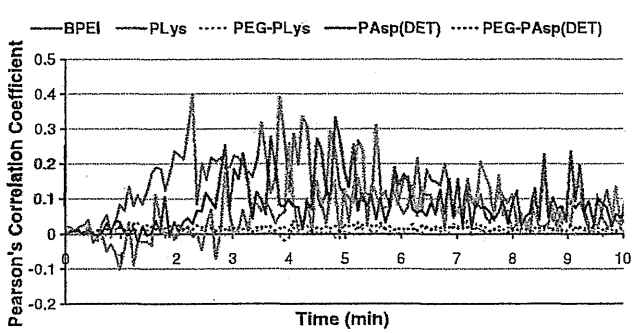

Fig. 3. Quantification of colocalization between polyplexes/micelles and platelets. The colocalization was measured with PCC. PCC was calculated from the frames extracted every 5 s from crude videos.

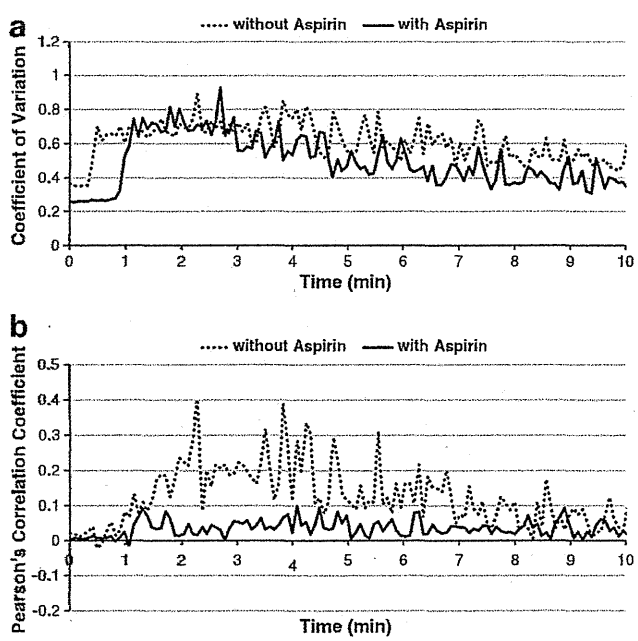

Fig. 4. Platelets inhibition study with aspirin. (a) Aggregates of BPEI/pDNA polyplexes of the aspirin-administered mouse was quantified with the CV of Cy5 fluorescence intensities in the frames extracted every 5 s from crude videos. (b) Colocalization between BPEI/pDNA polyplexes and platelets of the aspirin-administered mouse was quantified with PCC. PCC was calculated from the frames extracted every 5 s from crude videos. For comparison, the CV and PCC of the BPEI/pDNA polyplexes-administered normal mouse in Figs. 2 and 3 were shown respectively again.

of nonviral gene vectors. In the present study, the mouse earlobe was noninvasively fixed beneath the coverslip, and the vein was imaged at the dermis layer. Confocal imaging eliminated light from out-of-focus sections in the ear lobe such as the epidermis and hypodermis. Furthermore, we kept the confocal slice thinner (5.11 μm) than the diameter of the vein, so that the signal was detected only from inside the vasculature. High-speed scanning was essential to obtain unambiguous images to quantify the aggregates and colocalization between nonviral gene vectors and platelets because conventional galvano scanners are too slow to distinguish the individual aggregates and platelets rapidly flowing in the bloodstream, providing insufficient and blurred images (Supplementary Videos 7 and 8).

We investigated the polycations BPEI and PLys. They are widely used to construct polyplexes and PAsp(DET) has reduced cytotoxicity and high transfection efficiency [13]. To evaluate the improvement of biocompatibility via PEGylation, PEG-PLys/pDNA and PEG-PAsp (DET)/pDNA micelles were examined. A simple and effective way to PEGylate polyplexes is, as we reported [10–12], to use PEG-based cationic block copolymers as counterpart polycations to pDNA. The block copolymers are characterized by tandem alignment of a hydrophilic PEG segment and a cationic segment, leading to the formation of stable and biocompatible micelles with a core of polycation/pDNA complex surrounded by a dense PEG palisade and size of approximately 100 nm. Indeed, the micelle composed of PEG-PLys and pDNA achieved higher stability than that of unmodified PLys/pDNA polyplex in a medium containing serum and showed prolonged blood circulation [18,24]. The block copolymer possessing a cationic polyaspartamide segment carrying an ethylenediamine unit at the side chain, PEG-PAsp(DET), also formed the micelle with pDNA, which prevented nonspecific interaction with biological components such as erythrocytes and platelets under *in vitro* conditions [8].

IVRTCLSM was used to directly investigate the interaction between these gene vectors and platelets in the bloodstream. IVRTCLSM could be used to evaluate the dynamic states of nonviral gene vectors rapidly flowing in the bloodstream over time *in situ* (Fig. 1 and Supplementary Videos 1–6). This is the first report to visualize the formation of aggregates and the prevention by PEGlyation of polyplexes *in situ* in the bloodstream.

To quantify the aggregates, we adopted the CV. CV values reflected the nonuniform fluorescence distribution of polyplexes and uniform fluorescence distribution of micelles (Fig. 2). It is noteworthy that our IVRTCLSM started video acquisition 10 s before administration, allowing us to follow aggregate formation immediately after injection. CV values of the polyplexes rapidly increased approximately 20–30 s after injection, and corresponded well with the entry of polyplexes, indicating instantaneous formation of aggregates (Fig. 2). CV values also fluctuated over time, depending on the amount of aggregates at those time points. Furthermore, CV values of polyplexes decreased with time due to their disappearance from the bloodstream. In contrast, CV values of micelles were moderately elevated when micelles passed the ROI first. This moderate elevation was because of the admixture of micelles and blood without aggregate formation. Moreover, CV values were retained at a plateau after this moderate elevation, suggesting persistent circulation and uniform distribution of micelles in the bloodstream.

IVRTCLSM was also useful for the investigation of the dynamic interaction between nonviral gene vectors and platelets. Indeed, we succeeded in visualizing the interaction between polyplexes and platelets *in situ*. This dynamic information could not be revealed without IVRTCLSM.

To quantify the platelet interaction, we adopted PCC between polyplexes/micelles and platelets (Fig. 3). PCC values of polyplexes did not increase at the time point when CV values started to increase. PCC values began to increase after approximately 1 min after injection, and indicated strong correlation between polyplexes and platelets 2 min after injection. This temporal gap between aggregate formation and platelet interaction strongly indicated that aggregate formation was not triggered by platelets. To confirm this, we conducted the study in mice that were administered aspirin (Fig. 4). Aspirin induces a long-lasting functional defect in platelets [25], and thus may inhibit platelet interaction with polyplexes. The CV and PCC quantitatively demonstrated that oral administration of aspirin successfully inhibited platelet interaction with aggregates (Fig. 4b), but did not inhibit aggregate formation itself (Fig. 4a). This result indicates that the aggregate formation of polyplexes does not involve platelets (at least in the initial stage). Presumably, some protein components in plasma may have a role in aggregate formation, but further investigation is needed to clarify the mechanism.

Aggregate formation in the range of several micrometers immediately after intravenous injection should crucially affect the efficiency of systemically injected polyplexes. The aggregated polyplexes cannot extravasate into the targeted tissues or cells. Moreover, they might lead to thrombosis through the interaction with platelets to obstruct microvessels in normal tissue, including the lungs and liver, resulting in nonspecific accumulation of polyplexes in these tissues. This accumulation caused by aggregate formation will lead to unfavorable effects such as pulmonary embolism. The micelles, in contrast, did not form aggregates, and also showed no interaction with platelets. Thus, they are expected to prevent adverse effects caused by polyplex agglomeration, which cannot be inhibited even by oral administration of aspirin. This result confirms that PEGylation is a rational strategy to improve the biocompatibility of nonviral gene vectors based on polyplex formation [3,10–12].

In the present study, IVRTCLSM was used to visualize and quantify the dynamic states of polyplexes flowing in the bloodstream. Moreover, with respect to ethics, IVRTCLSM excels conventional *ex vivo* methods that involve the sacrifices of numerous animals to acquire pharmacokinetic information. IVRTCLSM provides temporal and spatial information at 30 time points in 1 s with a single mouse, which is desirable for high-throughput screening of newly developed DDSs.

In conclusion, IVRTCLSM was developed and applied to directly investigate the dynamic state of gene vectors in the bloodstream. Aggregate formation of the polyplexes and its prevention by PEGylation was observed *in situ* for the first time under the flow in the capillary. Thus, IVRTCLSM could provide the requisite information that has not been obtained by conventional methods, thereby giving a new facet in the research on systemic gene delivery.

Supplementary materials related to this article can be found online at doi:10.1016/j.jconrel.2011.02.011.

Acknowledgment

This work was supported in part by Core Research Program for Evolutional Science and Technology (CREST) from the Japan Science and Technology Corporation (JST) and Funding Program for World-Leading Innovative R&D on Science and Technology (FIRST Program) from Japan Society for the Promotion of Science (JSPS).

References

[1] D.W. Pack, A.S. Hoffman, S. Pun, P.S. Stayton, Design and development of polymers for gene delivery, Nat. Rev. Drug Discov. 4 (2005) 581–593.
[2] T. Merdan, K. Kunath, H. Petersen, U. Bakowsky, K.H. Voigt, J. Kopecek, T. Kissel, PEGylation of poly(ethylene imine) affects stability of complexes with plasmid DNA under in vivo conditions in a dose-dependent manner after intravenous injection into mice, Bioconjug. Chem. 16 (2005) 785–792.
[3] M. Ogris, E. Wagner, Targeting tumors with non-viral gene delivery systems, Drug Discov. Today 7 (2002) 479–485.
[4] Y. Kakizawa, K. Kataoka, Block copolymer micelles for delivery of gene and related compounds, Adv Drug Deliver Rev 54 (2002) 203–222.

[5] K. Osada, R.J. Christie, K. Kataoka, Polymeric micelles from poly(ethylene glycol)-poly(amino acid) block copolymer for drug and gene delivery, J. R. Soc. Interface 6 (2009) S325–S339.
[6] Y.Y. Yang, Y. Wang, R. Powell, P. Chan, Polymeric core–shell nanoparticles for therapeutics, Clin. Exp. Pharmacol. Physiol. 33 (2006) 557–562.
[7] M. Ogris, S. Brunner, S. Schuller, R. Kircheis, E. Wagner, PEGylated DNA/transferrin-PEI complexes: reduced interaction with blood components, extended circulation in blood and potential for systemic gene delivery, Gene Ther. 6 (1999) 595–605.
[8] D. Akagi, M. Oba, H. Koyama, N. Nishiyama, S. Fukushima, T. Miyata, H. Nagawa, K. Kataoka, Biocompatible micellar nanovectors achieve efficient gene transfer to vascular lesions without cytotoxicity and thrombus formation, Gene Ther. 14 (2007) 1029–1038.
[9] Y. Matsumoto, T. Nomoto, H. Cabral, Y. Matsumoto, S. Watanabe, R.J. Christie, K. Miyata, M. Oba, T. Ogura, Y. Yamasaki, N. Nishiyama, T. Yamasoba, K. Kataoka, Direct and instantaneous observation of intravenously injected substances using intravital confocal micro-videography, Biomed. Opt. Express 1 (2010) 1209–1216.
[10] K. Osada, R.J. Christie, K. Kataoka, Polymeric micelles from poly(ethylene glycol)-poly(amino acid) block copolymer for drug and gene delivery, J. R. Soc. Interface 6 (Suppl. 3) (2009) S325–339.
[11] Y. Kakizawa, K. Kataoka, Block copolymer micelles for delivery of gene and related compounds, Adv. Drug Deliv. Rev. 54 (2002) 203–222.
[12] N. Nishiyama, K. Kataoka, Current state, achievements, and future prospects of polymeric micelles as nanocarriers for drug and gene delivery, Pharmacol. Ther. 112 (2006) 630–648.
[13] K. Itaka, T. Ishii, Y. Hasegawa, K. Kataoka, Biodegradable polyamino acid-based polycations as safe and effective gene carrier minimizing cumulative toxicity, Biomaterials 31 (2010) 3707–3714.
[14] A. Harada, K. Kataoka, Formation of polyion complex micelles in an aqueous milieu from a pair of oppositely-charged block-copolymers with poly(ethylene glycol) segments, Macromolecules 28 (1995) 5294–5299.
[15] V. Zinchuk, O. Zinchuk, T. Okada, Quantitative colocalization analysis of multicolor confocal immunofluorescence microscopy images: pushing pixels to explore biological phenomena, Acta Histochem. Et Cytochem. 40 (2007) 101–111.
[16] K. Miyata, S. Fukushima, N. Nishiyama, Y. Yamasaki, K. Kataoka, PEG-based block catiomers possessing DNA anchoring and endosomal escaping functions to form polyplex micelles with improved stability and high transfection efficacy, J. Control. Release 122 (2007) 252–260.
[17] K. Kawabata, Y. Takakura, M. Hashida, The fate of plasmid dna after intravenous-injection in mice — involvement of scavenger receptors in its hepatic-uptake, Pharm. Res. 12 (1995) 825–830.
[18] M. Harada-Shiba, K. Yamauchi, A. Harada, I. Takamisawa, K. Shimokado, K. Kataoka, Polyion complex micelles as vectors in gene therapy — pharmacokinetics and in vivo gene transfer, Gene Ther. 9 (2002) 407–414.
[19] K. Kataoka, T. Tsuruta, T. Akaike, Y. Sakurai, Biomedical behavior of synthetic polyion complexes toward blood-platelets, Makromolekulare Chem. Macromol. Chem. Phys. 181 (1980) 1363–1373.
[20] T.K. Rosborough, Parallel inhibition of ristocetin and polycation-induced platelet agglutination, Thromb. Res. 19 (1980) 417–422.
[21] P. Chollet, M.C. Favrot, A. Hurbin, J.L. Coll, Side-effects of a systemic injection of linear polyethylenimine–DNA complexes, J. Gene Med. 4 (2002) 84–91.
[22] M.R. Dowling, E.C. Josefsson, K.J. Henley, P.D. Hodgkin, B.T. Kile, Platelet senescence is regulated by an internal timer, not damage inflicted by hits, Blood 116 (2010) 1776–1778.
[23] S. Hak, N.K. Reitan, O. Haraldseth, C. Lange Davies, Intravital microscopy in window chambers: a unique tool to study tumor angiogenesis and delivery of nanoparticles, Angiogenesis 13 (2010) 113–130.
[24] K. Itaka, K. Yamauchi, A. Harada, K. Nakamura, H. Kawaguchi, K. Kataoka, Polyion complex micelles from plasmid DNA and poly(ethylene glycol)-poly(L-lysine) block copolymer as serum-tolerable polyplex system: physicochemical properties of micelles relevant to gene transfection efficiency, Biomaterials 24 (2003) 4495–4506.
[25] C. Patrono, Aspirin as an antiplatelet drug, N. Engl. J. Med. 330 (1994) 1287–1294.

Neuroscience Letters 487 (2011) 12–16

Contents lists available at ScienceDirect

Neuroscience Letters

journal homepage: www.elsevier.com/locate/neulet

Hydrogen in drinking water attenuates noise-induced hearing loss in guinea pigs

Ying Lin [a], Akinori Kashio [b], Takashi Sakamoto [b], Keigo Suzukawa [b], Akinobu Kakigi [b], Tatsuya Yamasoba [b,*]

[a] Department of Otolaryngology and Head and Neck Surgery, Xijing Hospital, Xi'an, China
[b] Department of Otolaryngology and Head and Neck Surgery, University of Tokyo, Tokyo, Japan

ARTICLE INFO

Article history:
Received 14 July 2010
Received in revised form
17 September 2010
Accepted 23 September 2010

Keywords:
Temporary threshold shift
Oxidative stress
Cochlea
Hair cell

ABSTRACT

It has been shown that molecular hydrogen acts as a therapeutic and preventive antioxidant by selectively reducing the hydroxyl radical, the most cytotoxic of the reactive oxygen species. In the present study, we tested the hypothesis that acoustic damage in guinea pigs can be attenuated by the consumption of molecular hydrogen. Guinea pigs received normal water or hydrogen-rich water for 14 days before they were exposed to 115 dB SPL 4-kHz octave band noise for 3 h. Animals in each group underwent measurements for auditory brainstem response (ABR) or distortion-product otoacoustic emissions (DPOAEs) before the treatment (baseline) and immediately, 1, 3, 7, and 14 days after noise exposure. The ABR thresholds at 2 and 4 kHz were significantly better on post-noise days 1, 3, and 14 in hydrogen-treated animals when compared to the normal water-treated controls. Compared to the controls, the hydrogen-treated animals showed greater amplitude of DPOAE input/output growth functions during the recovery process, with statistical significance detected on post-noise days 3 and 7. These findings suggest that hydrogen can facilitate the recovery of hair cell function and attenuate noise-induced temporary hearing loss.

Exposure to loud noise may cause sensorineural hearing loss that can last for minutes, hours, days, or permanently, depending on the parameters of the acoustic overstimulation and the subject's susceptibility to noise exposure. Noise-induced temporary threshold shift (TTS) is a reversible elevation in hearing threshold that occurs after acoustic overstimulation. TTS can be an indicator of exposures that lead to permanent hearing loss after multiple, cumulative exposure events. Although the mechanisms underlying this phenomenon are not fully understood, it is widely accepted that direct mechanical damage and/or indirect metabolic alterations may be involved. Most notably, the generation of reactive oxygen species (ROS) [12], which may serve as triggers for necrosis or apoptosis, results in damage to the cochlear hair cells and the subsequent degeneration of auditory neurons. Thus, suitable antioxidants are desired to protect against oxidative damage in the inner ear. Pharmacological agents effective against TTS may have a potential clinical role in the prophylaxis of acute acoustic damage. However, most antioxidants have difficulty reaching the cochlear hair cells because of the blood–labyrinthine barrier.

Recent studies have revealed that molecular hydrogen mediates beneficial effects in different systems as an optimal antioxidant agent by selectively scavenging free hydroxyl radicals (•OH) [23,25]. Inhaled hydrogen gas can prevent or reduce pathological or biochemical changes in animal models of cerebral infarction [23], neonatal hypoxia ischemia [4], hepatic injury [9], intestinal ischemia injury [2], myocardial ischemia-reperfusion injury [11], cisplatin-induced nephrotoxicity [19], polymicrobial sepsis [26], and generalized inflammation [27]. Continuous consumption of hydrogen water can also protect against intestinal ischemia [29], neonatal hypoxia-ischemia [3], chronic allograft nephropathy [5] and acute pancreatitis [6]. It has also been shown to reduce atherosclerotic lesions in apolipoprotein E knock-out mice [24], inactivate oxidative stress in the brain of Parkinson disease rodents [7,8], and prevent stress-induced decline in learning and memory caused by chronic physical restraint [18]. Hydrogen-loaded eye drops can also protect the retina from ischemia-reperfusion injury [21]. A clinical study has shown that consuming hydrogen-rich water improves lipid and glucose metabolism in type 2 diabetes patients [14]. Furthermore, hydrogen-saturated culture medium can protect cochlear hair cells against antimycin A-induced oxidative stress *in vitro* [16].

Because of permeability and few side effects of molecular hydrogen, it is considered especially favorable as a component of inner-ear medicine. In the present study, therefore, we tested the

* Corresponding author at: Department of Otolaryngology and Head and Neck Surgery, Faculty of Medicine, University of Tokyo, Hongo 7-3-1, Bunkyo-ku, Tokyo 113-8655, Japan.
E-mail address: tyamasoba-tky@umin.ac.jp (T. Yamasoba).

0304-3940/$ – see front matter © 2010 Elsevier Ireland Ltd. All rights reserved.
doi:10.1016/j.neulet.2010.09.064